8-29-2020

Path Loss Model for 2.4GHZ Indoor Wireless Networks with Application to Drones

Rahul Gulia
rg9828@rit.edu

RIT

PATH LOSS MODEL FOR 2.4GHZ INDOOR WIRELESS NETWORKS WITH APPLICATION TO DRONES

by

Rahul Gulia

A Thesis Submitted in Partial Fulfillment of the Requirements for the Degree of Master of Science in Electrical Engineering

Electrical Engineering
Kate Gleason College of Engineering

Rochester Institute of Technology
Rochester, NY
August 29, 2020

Supervised by:

Dr. Gill R. Tsouri

PATH LOSS MODEL FOR 2.4GHZ INDOOR WIRELESS NETWORKS WITH APPLICATION TO DRONES

Approved by:

_____

Dr. Gill R. Tsouri
Primary Advisor – R.I.T. Dept. of Electrical & Microelectronic Engineering

_____

Dr. Jayanti Venkataraman
Director – R.I.T. Dept. of Electromagnetics Theory and Applications (ETA) Laboratory in the Electrical and Microelectronic Engineering Department

_____

Dr. Amlan Ganguly
Associate Professor and Interim Head – R.I.T. Department of Computer Engineering

_____

Dr. Ferat Sahin
Department Head – R.I.T. Dept. of Electrical & Microelectronic Engineering

ACKNOWLEDGEMENTS

I would like to thank my advisor Dr. Gill R. Tsouri, Professor of Electrical Engineering at Rochester Institute of Technology, for his guidance and support for this project. It was a great opportunity to learn from his experience and knowledge.

I would also like to thank my family and friends for their support. Without their continuous support I would not be able to come this far.

ABSTRACT

Indoor wireless communication using Wireless Fidelity (Wi-Fi) is becoming a major need for the success of Unmanned Aerial Vehicles (UAVs), Internet of Things (IoT) and cloud robotics in both developed and developing countries. With different operating conditions, interference, obstacles and type of building materials used, it is difficult to predict the path loss components in an indoor environment, which are crucial for the network design. It has been observed that the proposed indoor path loss models cannot be used for UAV operations due to variations in building materials utilized, floor plans, scattering on both ends, etc. In this work, we propose a non-deterministic statistical indoor path loss model, namely, the **UAV Low Altitude Air to Ground (U-LAAG)** model, adapted from ITU-R model, which can be used for the 2.4 - 2.5 GHz, Industrial Scientific and Medical (ISM) band. To test and validate the proposed model, we conduct several experiments with different conditions such as University premise with obstacles, typical dwelling and basement locations. We have also compared U-LAAG with popular path loss models such as ITU-R, Two-ray and Log-distance; U-LAAG matches closely with the drive test results as compared to other models. We believe that the proposed U-LAAG model can be used as basis to design accurate indoor communication networks required for regular Wi-Fi communications and deployment and operations of UAV, IoT and cloud robotics.

TABLE OF CONTENTS

LIST OF TABLES

LIST OF FIGURES

CHAPTER 1:
INTRODUCTION

UAV applications [22] offer civil and public domain applications in which single or multiple UAVs may be used. With the exponential increase in the application of Unmanned Aerial Vehicles (UAVs), in military as well as in commercial purposes [1], National Aerospace System (NAS) have taken active interest in regulating them in air. Control and Non-payload communication (CNPC) link specifications and dedicated communication links are designed to monitor and regulate each UAV operating in air. For each safe operation, an Air-Ground (AG) channel model must be modeled accurately for a UAV to serve its purpose in different terrains. The control of UAV will come mostly from ground stations (GS), and in some cases when the UAVs are operating in remote areas, high altitude antennas or satellites might be used.

Wireless communication has matured enough to become the de-facto mode of communication for the last couple of years. Considering Received Signal Strength Indicator (RSSI) as the measure of the Radio Frequency (RF) energy received by the receiver in our communication channel, as it is still being considered as the simplest open loop parameter for received signal strength measurement in practice. Hence, in this report we have used RSSI value as the measure of signal strength received at a receiver.

It has been observed that for an indoor environment, other than the transmission power and antenna gain, the materials used in the building, the building design pattern, equipment's used in the building and UAV's hovering location also impact heavily on the

RSSI values and their statistical distribution. This is because of the path loss occurring in such situations. Path loss needs to be modeled for optimal take-off and landing of UAVs from large and small distances. In this report, we concentrate only on the indoor scenario operation in 2.4 GHz band. Note that signal characteristics over 2.x GHz mainly depends upon multi-path propagation along with usual fading and path loss due to distance, interference, shadowing, scattering, reflection and refraction. In this direction, we assume a rich scattering environment near the base station (BS), as well as near to the UAV.

Accurately predicting the attenuation of a radio signal between two points in a realistic environment has many important applications in the design, rollout and maintenance of all types of wireless networks. Despite the large quantity of work done on modeling path loss, there is an important shortcoming that this work begins to address. Accurate model can help us understand the required power for a reliable connection, designing the link budget and ensure reliability in an indoor environment.

In this work, we compared various path loss models with our deterministic path loss model to ensure an optimized deployment of the UAVs in rich scattering environment. The model was not instantaneous, but rather an average path loss model created over 250 samples. Average Path loss model obtained by this work can be used to reduce the cost of deployment and operation, improved Quality of Service (QoS) in terms of un-interrupted data transmissions, high data rates, optimal transmission power, etc.

The remaining of the work is presented as follows. In Chapter 2, we discuss about the existing indoor modeling techniques. In Chapter 3 we propose our new model (U-LAAG). Chapter 4 presents the hardware and experiment setup to achieve an error-free data. Chapter 5 discusses on the measurement methodology, and the measured data is analyzed in Chapter 6. The new model parameters are discussed in Chapter 7, followed by the conclusions drawn in Chapter 8. And Chapter 9 discusses on the Future Work.

Our results for the scenario show that our proposed model approach leads to a significantly better channel model with considerable amount of accuracy when compared to other existing models. Thus, achieving a better planned power consumption link budget for reliable communication.

CHAPTER 2:
EXISTING INDOOR MODELING TECHNIQUES

Several indoor propagation models were proposed in the past. One-slope propagation model [2], general path loss model tested in a large number of indoor environment [3] and industrial sites [4]. An extension of one-slope model with better accuracy was introduced by authors in [5] as dual-slope model. Authors in [6],[7] have proposed indoor propagation models with lower prediction errors and have analyzed the correctness of their models through drive tests. Their analysis was performed for a site-specific validation of the ITU indoor path loss model such as indoor office environments and indoor airport area. In [8], authors have evaluated and examined the ITU based indoor path loss model for office and residential areas. Authors in [9] have considered Line of Sight (LOS) as well as non-LOS (NLOS) measurements to fit to a one-slope indoor propagation model. The authors have also considered the path loss exponents for wall losses in case of NLOS measurements.

From various studies, it is evident that the indoor environment is significantly different from the outdoor environment in many ways. Indoor path loss models need to consider the variations in the floor plans, construction materials used in the building, type and number of office equipment's used, number of people working and their movements,

scale of smart devices used in the vicinity, etc. Apart from these, multi-path propagation along with usual fading and path loss due to distance, interference, shadowing, reflection, refraction, scattering, and penetration etc., also impact on the received signal characteristics.

Despite a plethora of past work on channel models, we are still lacking the knowledge of UAV AG channel at very low altitudes, where the UAV might experience the same amount of scattering compared to a GS. So, it is crucial for UAV AG simulation models to consider the scatters around the UAV too. Considering the scenario of UAV at low altitude AG (U-LAAG) model, not much work was published in the area of UAV take-off and landing scenarios. So, a stochastic path loss (PL) fading model will be proposed for such cases based on a measurement campaigns, and it will be compared to the various proposed models like PL 2-ray model, Log-distance model and PL ITU-R model, to measure the accuracy of our model.

2.1 Two-ray Path Loss model

When a reflected ray exists besides the LOS components, the propagation loss can be predicted by a two-ray loss model as in [10]. The two-ray ground reflection model considers both the direct path and a ground reflection path. It is shown that this model gives more accurate prediction at a long distance (above 6m in our case) than the free space path loss model. The received power at distance *d* is predicted by

$$P_r(d) = \frac{\mathrm{P}_t \mathrm{G}_t \mathrm{G}_r \mathrm{h}_t^2 \mathrm{h}_r^2}{\mathrm{d}^4 \mathrm{L}} \tag{2.1}$$

Where h_t and h_r are the heights of the transmit and receive antennas, respectively. Note that the original equation assumes $L = 1$. To be consistent with the free space model, L is added here.

The above equation shows a faster power loss than the Free Space path loss model as distance increases. However, the two-ray model does not give a good result for shorter distances due to the oscillation caused by the constructive and destructive combination of the two rays.

The authors in [11] presented an experimental study of air-to-ground channels over sea surface at the C-band (5.7 GHz) with low airborne altitudes through wideband channel measurements. The multipath statistics and the propagation loss at different

airborne altitudes are estimated and analyzed. It was observed that 86% of the measured channel responses can be represented by the two-ray multipath model, and as the airborne altitude decreases, there is a higher probability for the appearance of multipath components. And these were few of the reasons for me to compare my model with the two-ray path loss model.

2.2. Log-Distance Path Loss model

Frii's free space propagation model is used to model the LOS path loss incurred in a free space environment, devoid of any objects that create absorption, diffraction, reflections, or any other characteristic-altering phenomenon to a radiated wave. It is valid only in the far field region of the transmitting antenna [19] and is based on the inverse square law of distance which states that the received power at a particular distance from the transmitter decays by a factor of square of the distance. The Frii's equation for received power is given by

$$P(d) = \frac{P_t G_t G_r \lambda^2}{(4\pi)^2 d^2 L} \tag{2.2}$$

P(d): received power with the distance d
P_t: transmitted power
λ: wavelength of the carrier
G_t , Gr: antenna gains
L: loss factor

Log-distance path loss model [12] is a generic model and an extension to Frii's Free space model. Both theoretical and measurement based propagation models indicate that average received signal power decreases logarithmically with distance, whether in outdoor or indoor radio channels. It is used to predict the propagation loss for a wide range of environments, whereas, the Frii's Free space model is restricted to unobstructed clear path between the transmitter and the receiver.

In the far field region of the transmitter ($d \geq d_f$), if PL(d_o) is the path loss measured in dB at a distance d_0 from the transmitter, then the path loss (the loss in signal power measure in dB when moving from distance d_o to d) at an arbitrary distance $d > d_o$ is given by

$$\overline{PL}(dB) = \overline{PL}(\mathrm{d}_0) + 10.n.log\ (\frac{d}{d_0}) \qquad (2.3)$$

The average path loss is expressed as a function of distance by using a path loss exponent, n, which indicates the rate at which the path loss increases with distance d_o is the close-in reference distance which is determined from measurements close to the transmitter and d is the Transmitter-Receiver separation distance. Table 2.1 below gives the path loss exponent for various environments.

Environment	Path Loss Exponent (n)
Free Space	2
Urban area cellular radio	2.7 to 3.5
Shadowed urban cellular radio	3 to 5
Inside a building – Line of Sight	1.6 to 1.8

Obstructed in building	4 to 6
Obstructed in Factory	2 to 3

Table 2.1 Path Loss exponent

2.3 ITU-R model

The ITU indoor propagation model, also known as ITU model for indoor attenuation, is a radio propagation model that estimates the path loss inside a room or a closed area inside a building delimited by walls of any form. Suitable for appliances designed for indoor use, this model approximates the total path loss an indoor link may experience.

$$PL(dB) = 20\log_{10} f + N\log_{10} d + P_f(n) - 28 \qquad (2.4)$$

PL (dB): the total path loss.
f (MHz): Frequency of transmission.
d (m): Distance.
N: distance power loss coefficient.
n: Number of floors between the transmitter and receiver.
$P_f(n)$: floor loss penetration factor.

The distance power loss coefficient, N is the quantity that expresses the loss of signal power with distance. This coefficient is an empirical one. Its values are tabulated in Table 2.2. The floor penetration loss factor is an empirical constant dependent on the number of floors the waves need to penetrate. Its values are tabulated in Table 2.3.

Frequency Band	Residential Area	Office Area	Commercial Area
900 MHz	M/A	33	20
1.2-1.3 GHz	N/A	32	22
1.8-2 GHz	28	30	22
4 GHz	N/A	28	22
5.2 GHz	N/A	31	N/A

Table 2.2 Power Loss Coefficient Values, N, for the ITU Model

Frequency Band	No. of Floors	Residential Area	Office Area	Commercial Area
900 MHz	1	N/A	9	N/A
900 MHz	2	N/A	19	N/A
900 MHz	3	N/A	24	N/A
1.8-2.0 GHz	1-3	4n	15+4(n-1)	6+3(n-1)
5.2 GHz	1	N/A	16	N/A

Table 2.3 Floor Penetration Loss Factor, $P_f(n)$, for the ITU Model

The authors in [13], [14] have proposed indoor propagation models with lower prediction errors and have analyzed the correctness of their model through drive tests. Their analysis was performed for a site-specific validation of the ITU indoor path loss model such as indoor office environments [13] and indoor airport area. In [15], authors have evaluated ITU based indoor path loss model and have examined whether ITU model can be used in office or residential areas. However, these experiments use high-end circuits and hence are not cost effective methods for other types of indoor environments.

CHAPTER 3:
PROPOSED MODEL

3.1 Proposed Model: UAV at Low Altitude AG Model (U-LAAG)

Since we are interested in developing a path loss model for the 2.4 GHz band in an indoor scenario for take-off and landing of a UAV, we have conducted several drive tests in a typical indoor environment with various conditions and constraints.

Our proposed model is an empirical deterministic statistical model named as UAV at Low Altitude AG (U-LAAG) model. Using curve fitting mechanisms and adapting from the ITU-R model, we propose our path loss model - UAV at Low Altitude AG (U-LAAG) model as:

$$PL_{U-LAAG}(dB) = 20 * A * \log_{10} f_c + B * \log_{10} d + C + X_{sigma} \quad (3.1)$$

where, *A* & *B* are constant coefficients, indicating effects of frequency and distance on PL. *C* is the offset in PL. X_{sigma} is the zero-mean Gaussian distributed random variable with standard deviation 'sigma'.

From the experiment results, we have observed that the popular ITU-R model differs significantly from our drive test data till a threshold distance ($d_{threshold}$). Therefore,

we have attempted to propose a path loss model which can be used for regular operations in a UAV take-off and land scenarios for closer distances.

Indoor path loss models like Two-ray, Log-distance and ITU-R are used for comparison. All the models discussed in previous chapter are successful in predicting the attenuation for a UAV at higher altitudes, but they failed to do so in a typical UAV take-off and landing scenario at low altitudes. Two-ray and Log-distance path loss models had the maximum deviation from the mean observed path loss when compared with ITU-R model.

In the following sections, we describe our measurement campaign, the model fitting results for each one of the models described above and our rational for the U-LAAG model based on our observations.

CHAPTER 4:
HARDWARE AND EXPERIMENT SETUP

4.1 Hardware

Digi Xbee3 RF modules are used for device connectivity and ZigBee-based mesh networking. Digi's Xbee 3 Mesh kit uses XBee modules which are small radio frequency (RF) devices to create mesh network that transmit and receive data over the air using ZigBee protocol, specifically designed for low-data rate and low-power applications. The device supports many applications such as remote control, long distance sensor monitoring, complex robotic, WAN, etc. The main advantage is low power consumption and simple developments.

Authors in [16] found its application in environmental monitoring scenarios like soil moisture control and temperature and humidity control. A variety of sensors in the plant, soil moisture, air quality, air temperature and humidity information were received from the Xbee end device. And a project in [17], centered on the development of a Wi-Fi integrated smart home system with a PIC® microcontroller and a Wi-Fi module as the core components was created. The developed Wi-Fi integrated smart home system was presented in the form of a smart room model, fully furnished and wired.

Digi XBee products have variety of products and models, which differ in size, protocol, operating frequency, and performance. XBee is divided into RF modules and cellular modules. Table 4.1 shows the specifications of basic XBee 3 and XBee 3 Pro. Both models use IEEE 802.15.4 ZigBee protocol. The major difference is enhanced performance of Pro model over basic model. In this project, basic XBee 3 RF modules are chosen to best fit the requirement.

	XBee 3	XBee 3 Pro
Indoor Range	60m (200 ft)	90m (300 ft)
Outdoor Range	1200m (4000 ft)	3200m (2 miles)
Transmit Power	+8 dBm	+19 dBm
Transmit Current	40 mA	135 mA
Supply Voltage	2.1 to 3.6 V	2.1 to 3.6 V

Table 4.1 Comparison of Xbee 3 and Xbee 3 Pro

XBee Zigbee Mesh Kit Components

XBee Zigbee Mesh kit main components are shown in figure 4.1. The kit includes 3 Digi Xbee Grove Development Boards, 3 Digi XBee 3 Zigbee SMT modules, 3 Micro-USB Cables and 3 Antennas.

Figure 4.1: Digi XBee Zigbee Mesh Kit Components

XBee Grove Development Board

XBee Grove Development Board is an easy simple base unit that allows user to evaluate XBee modules with PC or microcontroller. The grove development board can be powered by 5V supply using micro USB or external battery connected to the 2-pin battery pin. The board also provides a 3.3V regulator with 500mA. This development board has features such as several grove connectors and some push button. Grove connector pinout can be found in Appendix-A.

XBee3 ZigBee Surface Mount Module

XBee3 ZigBee SMT module is a low cost, low power, simple-to-use product that has 37 pads mounted directly to PCB without any pin holes. The ZigBee protocol has a frequency of 2.4GHz open global wireless standard with reliable communication through

noisy RF environments. We can use it to evaluate XBee modules, as it connects any XBee/XBee-PRO module to a PC or microcontroller. One of the main features of the board is that it has several Grove connectors where you can plug in a Grove Module. The module provides 4 10-bit ADC inputs and 15 digital I/O pins. The sight of range for this module is 200ft (60m) indoor and 4000ft (1200m) outdoor. The RF data rate is 250 kbps. The current draw for transmit is 40 mA @ 8 dBm and 17mA for receive. Pinout of XBee3 ZigBee SMT module can be found in Appendix-B.

Figure 4.2: XBee module mount on grove development board

Antenna

Antenna for 2.4 GHz with half wavelength dipole connect to XBee module for wireless communication between modules.

Figure 4.3: Half wavelength antenna

4.2 XBee Transmission Modes

Xbee 3 acts as RF device to communicate with other devices over air. Both devices must in the same network for successful transmission. XBee module support two operating modes, Transparent and Application Programming Interface (API) mode.

API mode provides the ability to perform more complex communication compared to transparent mode. It provides structured data communication by organizing packets into a frame. API mode can configure host or remote device through API frame, manage transmission to multiple remote device, status of transmit frame and request RSSI value of any received packet from any remote device. Figure 4.4 show that a coordinator is sending an AT command (0x17) request to read the remote device parameters, and the remote device is responding to AT command request (0x97) with the requested parameters.

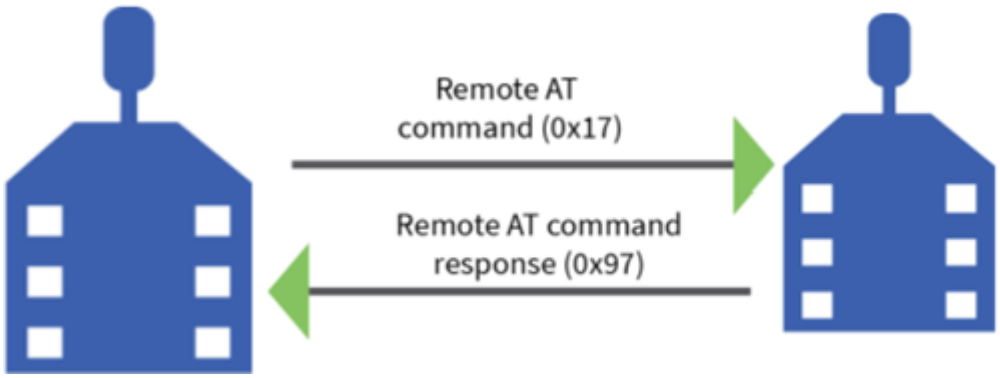

Figure 4.4: Request and Transmit through API mode

API Frame

In API mode, multiple packets information is structured together into an API frame. This frame is used to send and receive data through wireless communication. Some extra information added into API frame is start delimiter, checksum, destination and sources of the data. Start delimiter is the first byte of the frame to indicate start of the frame to make it easier to detect and separate between frames. Length shows the total number of bytes in the data frame. Data frame is the data information with source MAC address added. Check sum is the last byte in the frame to detect any error that occurs during transmission and reception. Table 4.2 shows the general example of the API frame. Table 4.3 shows the example of request AT command for RSSI value.

Start delimiter	Length		Frame data								Checksum
			Frame type	Data							
1	2	3	4	5	6	7	8	9	...	n	n+1
0x7E	MSB	LSB	API frame type	Frame-type-specific data							Single byte

Table 4.2: General API frame

Output	Field	Description
7E	Start Delimiter	Indicates the beginning of an API frame
0010	Length	Length of the packet
97	Frame type	Remote AT Command response frame

01	Frame ID	This ID corresponds to the Frame ID of the 0x17 request
0013A20041AAC8E8	64-bit source	The 64-bit address of the node that responded to the request
E5F5	16-bit source	The 16-bit address of the node that responded to the request
6462	AT Command	Indicates the AT command that this response corresponds to **DB**
00	Status	Indicates success or failure of the AT command **00** = **OK** if no I/O lines are enabled, this will return **01** (ERROR)
1E	Data sample	RSSI value in Hex
59	Checksum	Can safely be discarded on received frames

Table 4.3: Detailed remote AT command frame

RSSI as a Path Loss Indicator

Received Signal Strength Indicator (RSSI) measures power in the received signal. Since RSSI constantly changes in wireless communication channel based on the Transmitter-Receiver distance, scattering objects or the location of the end device, it is important to build a reliable WAN.

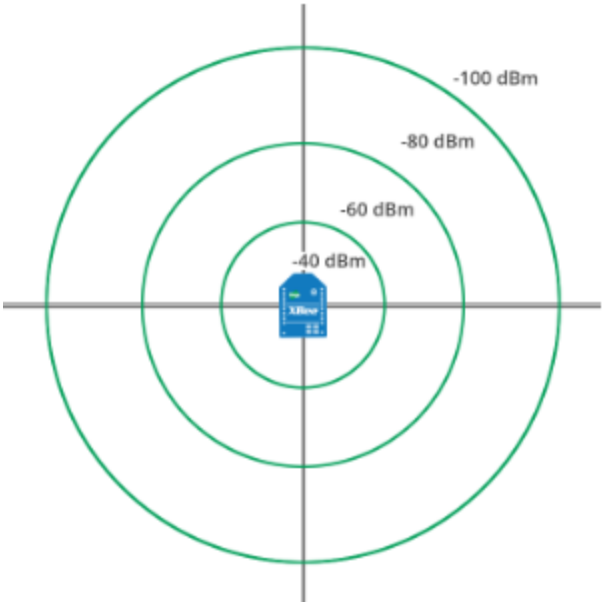

Figure 4.5: RSSI measurement in dBm

RSSI Principle

Frii's free space propagation model is used to model the LOS path loss incurred in a free space environment, devoid of any objects that create absorption, diffraction, reflections, or any other characteristic-altering phenomenon to a radiated wave. It is valid only in the far field region of the transmitting antenna [19] and is based on the inverse square law of distance which states that the received power at a particular distance from the transmitter decays by a factor of square of the distance. The Frii's equation for received power is given by

$$P(d) = \frac{\mathrm{P}_t \mathrm{G}_t \mathrm{G}_r \lambda^2}{(4\pi)^2 \mathrm{d}^2 \mathrm{L}} \tag{4.1}$$

P (d): is the received power with the distance d

P_t: transmitted power

λ: wavelength of the carrier

G_t, G_r: antenna gains

L: loss factor

Log-distance path loss model is an extension to the Frii's free space model. It is used to predict the propagation loss for a wide range of environments. The model encompasses random shadowing effects due to signal blockage by hills, trees, buildings etc. The path loss model is given by,

$$\overline{PL}(dB) = \overline{PL}(\mathrm{d}_0) + 10.n.log\ (\frac{d}{d_0}) \quad (4.2)$$

d_0: reference distance

n: path loss factor

With the reference distance d_0 = 1m. The signal transmission attenuation formula can be expressed as,

$$RSSI = A - 10.n.log(d) \quad (4.3)$$

where A is the received signal strength at reference distance 1m.

4.3 Experimentation

XBee 3 provides high data rate, good capacity of penetration through walls, low radiation and low energy consumption [20]. To fully simulate a real WAN, measurements are conducted with one XBee as coordinator (receiver) and another one as remote device (transmitter). The RSSI values measured are provided by XCTU software. RSSI can be used for path loss modeling, localization and channel characterization [21].

Experimental Setup

Figure 4.6: Experimental setup in lab

Our experiments were conducted in a lab to evaluate a series of measurements. The signals are measured by requesting RSSI through remote AT command. Both devices are first connected to PC through USB cable for initial configuration to form a wireless network as show in table 4.4. The coordinator device stays directly connected to PC for easier adjustment by XBee Configuration Test Utility (XCTU). The remote device is disconnected from PC to the wall outlet with approximate 3 ft apart from coordinator. The test setup is show in figure 4.6.

Parameter	XBee 1	XBee 2	XBee 3	Comment
JV	Disenable	Enabled [1]	Enabled [1]	Check for exists coordinator and ask to join the network
CE	Enabled [1]	Disenable	Disenable	Set the device as coordinator
AP	Enabled [1]	Enabled [1]	Enabled [1]	Enables API modes
NI	Coordinator	End device	End_device2	Name each XBee

Table 4.4: XBee Configuration

Experiment Procedure

For the experiment, we use XCTU to generate the requested AT command (0x17) for RSSI from the remote end device as shown in figure 4.7. This is a unicast message for remote end device. The coordinator sends a request AT command that was generated, and the remote end device receives it and sends the AT command response (0x97) back to the coordinator. The coordinator will detect the incoming data and record it into log file. To better simulate real life scenario, a vertical movement is made on remote end device to obtain the randomness of wireless network in real life situation. Total of 500 measurements are taken with packet interval time of 200ms [21]. Figure 4.8 shows the transmitted and received frame in XCTU.

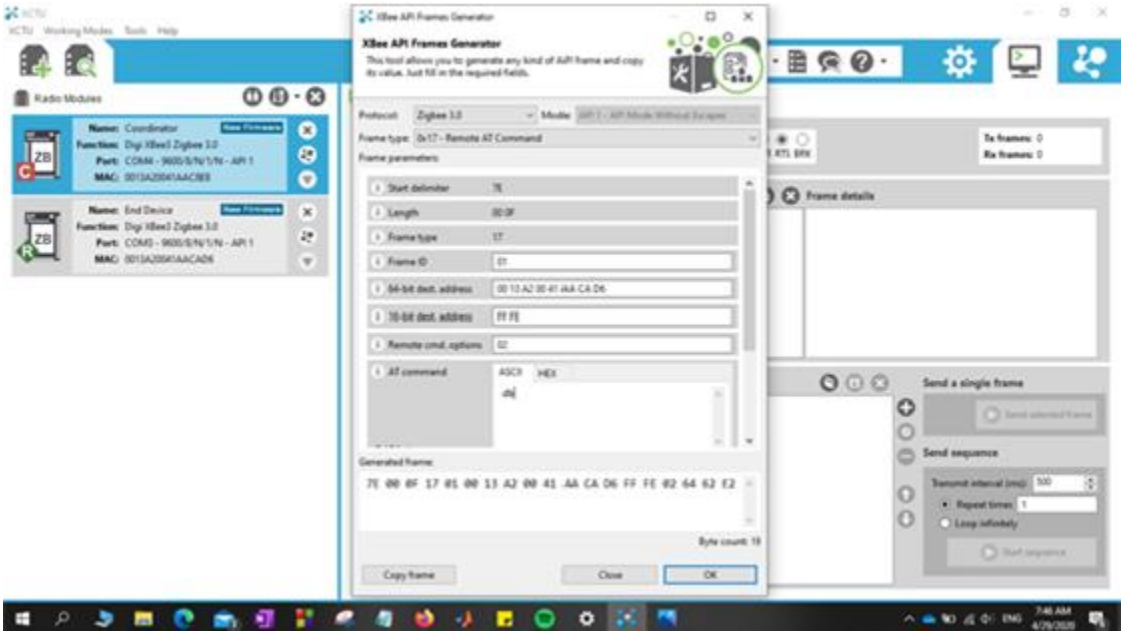

Figure 4.7: generate request AT command

Figure 4.8: received and transmit frame

RSSI Capture Results

A sample of the recorded result is show in figure 4.9. Notice the recorded frame data is in the order of request AT command send then AT command respond. This indicates a successful transmission between devices. Received frame structure details are described in section 3.2.3. The RSSI measured value is last 2 bytes before checksum. A MATLAB application was developed to make the result useable for future experiment. Load this raw sample data into MATLAB application to obtain RSSI vs. time plot and a table. The application also gives a .csv file with RSSI vs. time table as show in figure 4.10. Mathematical calculation of RSSI is shown in equation 3.3 above. Notice the randomness of RSSI plot due to movement in an indoor environment with obstacles.

```
02-25-2020 16:36:55.538,-,API,"Coordinator ,0013A20041AACAD6,Digi XBee3 Zigbee 3.0,1009,COM4 - 9600/8/N/1/N,0,65"

02-25-2020 16:36:57.411,291,SENT,7E000F17010013A20041AAC8E8FFFE02462D2
02-25-2020 16:36:57.481,292,RECV,7E00109701001 3A20041AAC8E8E5F56462001E59
02-25-2020 16:36:57.912,293,SENT,7E000F17010013A20041AAC8E8FFFE02462D2
02-25-2020 16:36:57.977,294,RECV,7E00109701001 3A20041AAC8E8E5F56462001E59
02-25-2020 16:36:58.413,295,SENT,7E000F17010013A20041AAC8E8FFFE02462D2
02-25-2020 16:36:58.522,296,RECV,7E00109701001 3A20041AAC8E8E5F56462001A5D
02-25-2020 16:36:58.914,297,SENT,7E000F17010013A20041AAC8E8FFFE02462D2
02-25-2020 16:36:58.989,298,RECV,7E00109701001 3A20041AAC8E8E5F56462001661
02-25-2020 16:36:59.414,299,SENT,7E000F17010013A20041AAC8E8FFFE02462D2
02-25-2020 16:36:59.486,300,RECV,7E00109701001 3A20041AAC8E8E5F56462001B5C
02-25-2020 16:36:59.915,301,SENT,7E000F17010013A20041AAC8E8FFFE02462D2
02-25-2020 16:36:59.994,302,RECV,7E00109701001 3A20041AAC8E8E5F56462002255
02-25-2020 16:37:00.416,303,SENT,7E000F17010013A20041AAC8E8FFFE02462D2
02-25-2020 16:37:00.500,304,RECV,7E00109701001 3A20041AAC8E8E5F56462001C5B
02-25-2020 16:37:00.917,305,SENT,7E000F17010013A20041AAC8E8FFFE02462D2
02-25-2020 16:37:01.005,306,RECV,7E00109701001 3A20041AAC8E8E5F56462002552
02-25-2020 16:37:01.417,307,SENT,7E000F17010013A20041AAC8E8FFFE02462D2
02-25-2020 16:37:01.512,308,RECV,7E00109701001 3A20041AAC8E8E5F56462002750
02-25-2020 16:37:01.917,309,SENT,7E000F17010013A20041AAC8E8FFFE02462D2
02-25-2020 16:37:02.028,310,RECV,7E00109701001 3A20041AAC8E8E5F5646200294E
02-25-2020 16:37:02.417,311,SENT,7E000F17010013A20041AAC8E8FFFE02462D2
02-25-2020 16:37:02.493,312,RECV,7E00109701001 3A20041AAC8E8E5F56462002453
02-25-2020 16:37:02.919,313,SENT,7E000F17010013A20041AAC8E8FFFE02462D2
02-25-2020 16:37:02.996,314,RECV,7E00109701001 3A20041AAC8E8E5F5646200185F
02-25-2020 16:37:03.419,315,SENT,7E000F17010013A20041AAC8E8FFFE02462D2
02-25-2020 16:37:03.541,316,RECV,7E00109701001 3A20041AAC8E8E5F56462001F58
```

Figure 4.9: sample of received frame

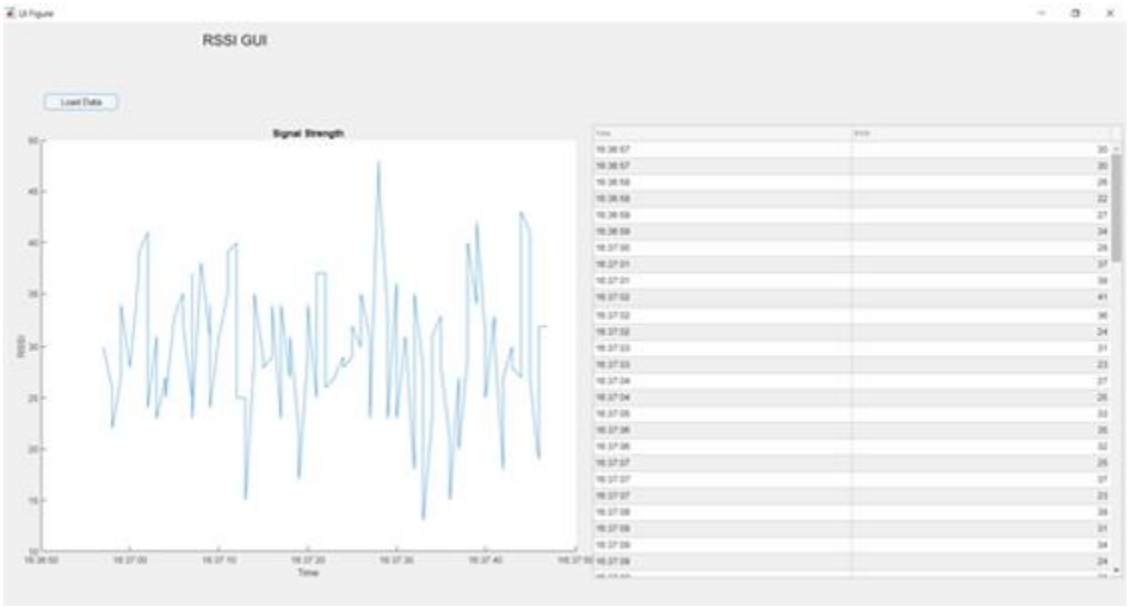

Figure 4.10: RSSI plot and table

CHAPTER 5:
MEASUREMENT METHODOLOGY

5.1 Measurement Setup

An optimized path loss technique was implemented for channel sounding at the transmitter. In our measurements, a unicast transmission was done, consisting of sending messages to a single node on the network identified by a unique address. Wireless data was addressed using the 64-bit address (network address). The ZigBee network layer uses the 64-bit address of the destination on each hop to route the data. API mode was used to have more flexibility and reliability in our data transmissions. In API mode, we could still send the message to the module. But, we also sent other necessary information, such as the destination address or checksum value, all wrapped in a packet with a defined structure called an API frame.

In our measurement, a transmit interval time of 500ms and repeat time of 250 times was configured. The transmission was secured by a Standard ZigBee security model which adds a number of optional security enhancements over residential security, including an APS layer link key. ZigBee security is applied to the Network and APS layers, and packets are encrypted with 128-bit AES encryption. A network key and optional link key were used to encrypt data. Only devices with the same keys are able to communicate together in a network.

We carried out the measurement setup in different types of indoor environments as shown in figure 5.1 – 5.3 to measure the signal attenuation

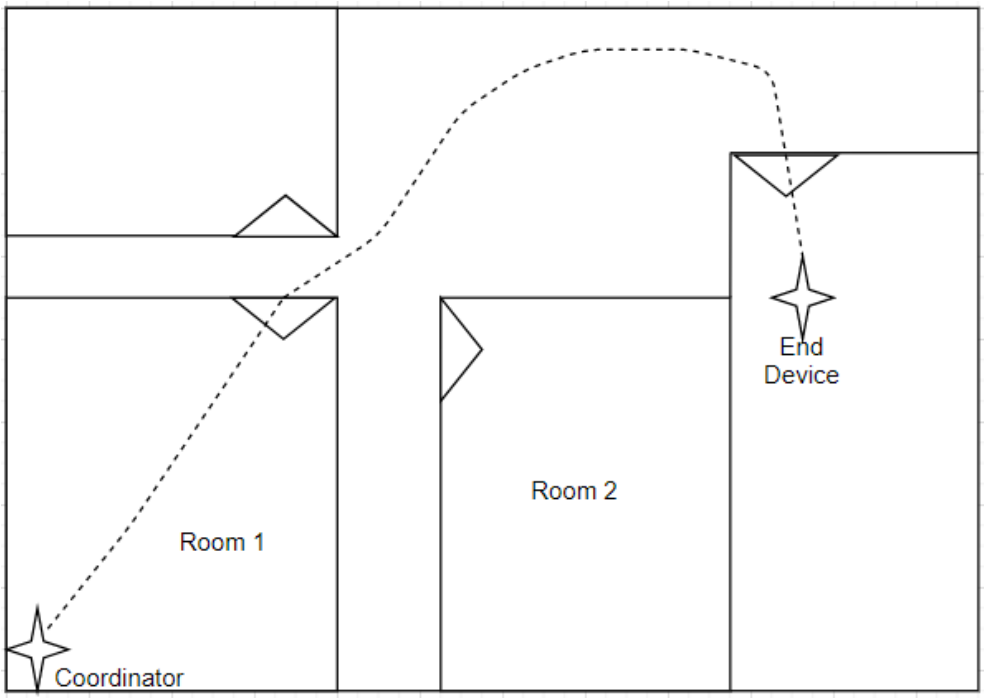

Figure 5.1: House layout (21x32 ft)

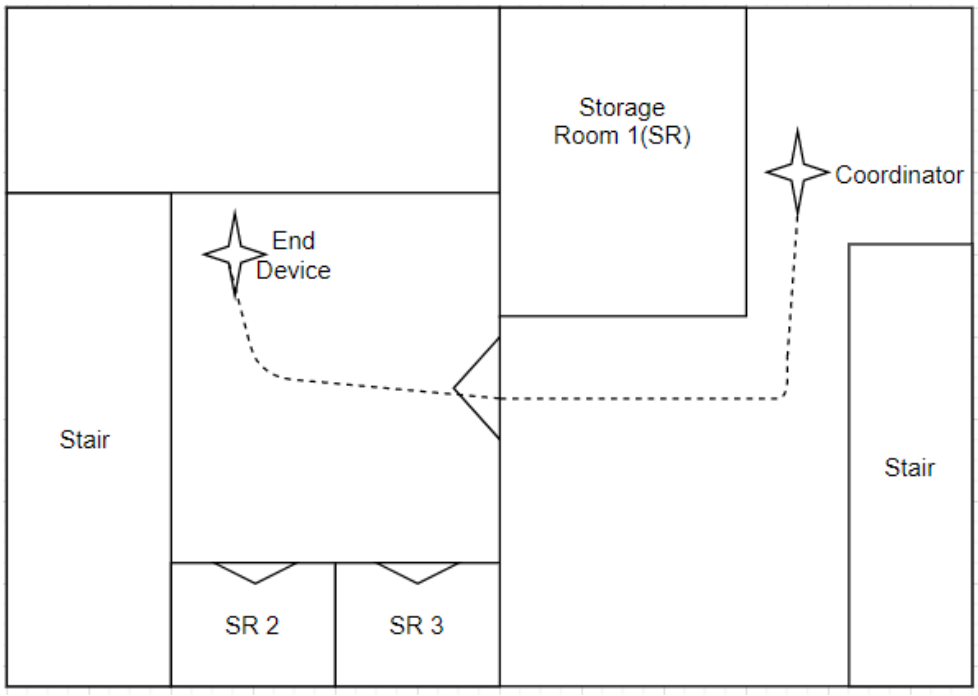

Figure 5.2: Basement layout (63 x 32 ft)

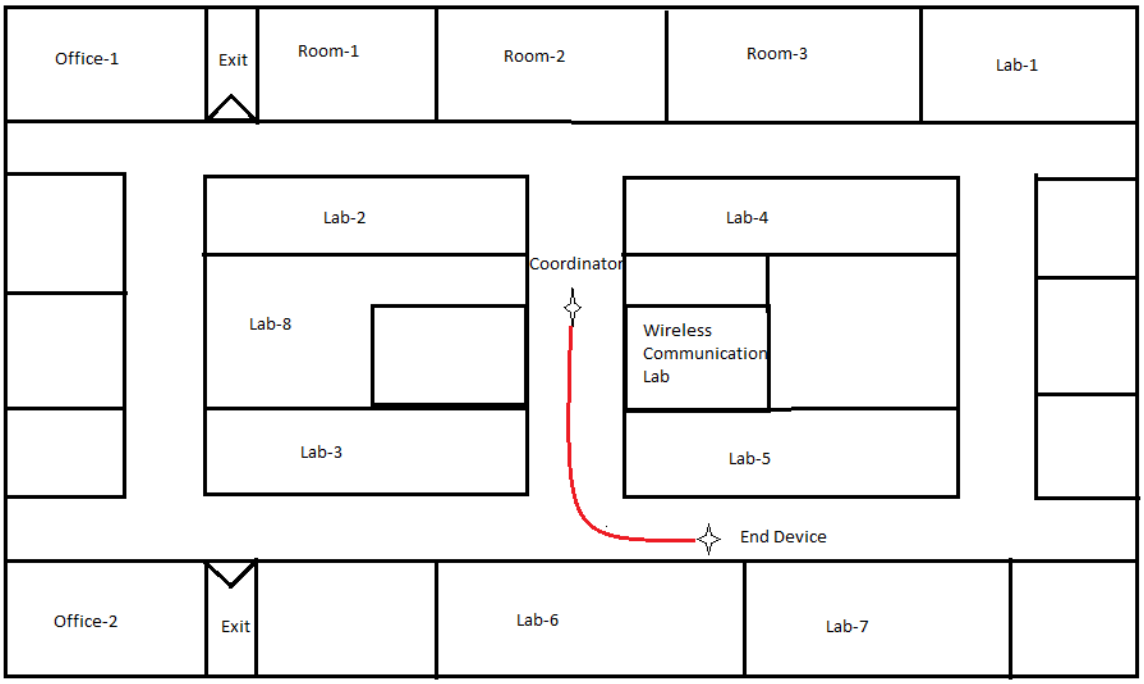

Figure 5.3: University layout (Corridor) (45 x 60 ft)

5.2 Measurement Procedure

Wideband air-to-ground channel measurements with low airborne altitudes were conducted in an indoor environment at 2.4 GHz. The radio wave mainly propagated in house, basement and various University locations. It was ensured that there was no LOS path between the transmitter and receiver. In this report, the radio-wave propagation along the flight paths, as illustrated in Fig 5.1 - 5.3 was investigated with a lot of scattering around both transmitter and receiver.

The coordinator was connected to PC for easier configuration in XCTU, acting as a remote control for our UAV. Coordinator is held at a constant vertical distance of 1m above the ground. The end device, acting as a UAV, is held in hand at distances ranging from 1m to 13m. The measurements were taken at distance ranging from 1m to 13m,

consisting of 250 samples at each location. Table 5.1 shows the accurate distance between transmitter and receiver at which the 250 samples were taken. The end device was moved vertically from 0m to 1.5m above the ground at a constant speed, imitating the take-off and landing scenario of a UAV, as shown in Fig 5.4.

Home Layout distance (m)	Basement Layout distance (m)	University Layout distance (m)
1	1	1
2	2.05	2
3	3.07	3
4	4.08	4
4.9	5.05	5
5.7	6.19	6
6.62	7.16	7
7.56	8	8
8.7	8.9	9.04
9.44	9.98	9.90
10.46	11.17	10.5
11.48	11.7	10.71
12.6	12.7	11.04
13.4	13.1	11.43
13.30	13.61	12.19

Table 5.1: Accurate measurement distance between Transmitter and Receiver

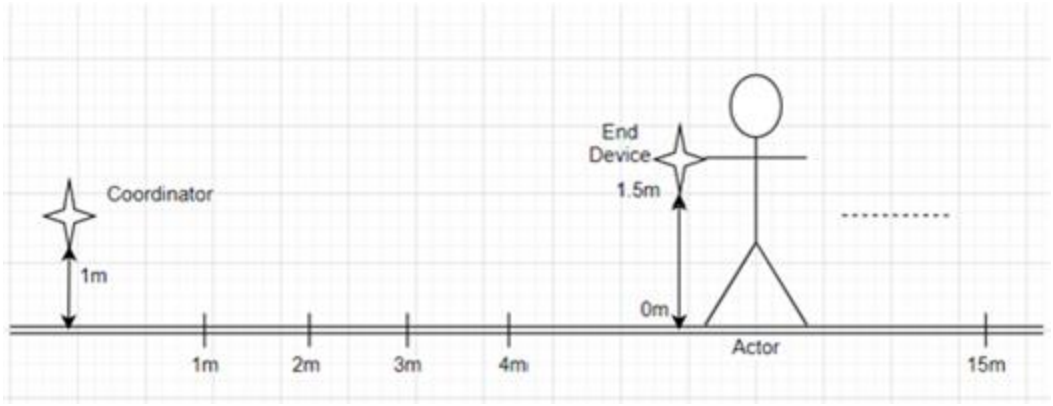

Figure 5.4: Test Procedure

We repeated the same experiment for about a week and have collected the RSSI values at multiple locations (with different Transmitter and Receiver placement) in in crowd less scenarios. We have noted the min, max and the mean values of the path loss values being observed at each location. From this, we have observed that mean or average path loss value measured can be used as an indicator for path loss modeling.

5.3 Measured Data samples

The experiment takes 250 samples at distance from 0 to 13m. Samples of RSSI are shown in the beginning at 1m, halfway at 7m, and the end at 13m of the measurement. A graphical plot is show in figure 5.8 – 5.10 for 250 samples. Different models are used to compare with experimental measurement. The experimental measurements are very close to ITU-R model in beginning and end of the measurement conducted in house for an optimized values of N = 22.8 and P_f = -127.28. The model intersects properly with our mean path loss model above 6m distance. For basement experiment, experimental measurements intersect with ITU-R model after a distance of

8m. This shows the ITU-R path loss model is the optimized model for our experiment after a certain minimum distance when compared to Log-Distance path loss model and 2-ray path loss model.

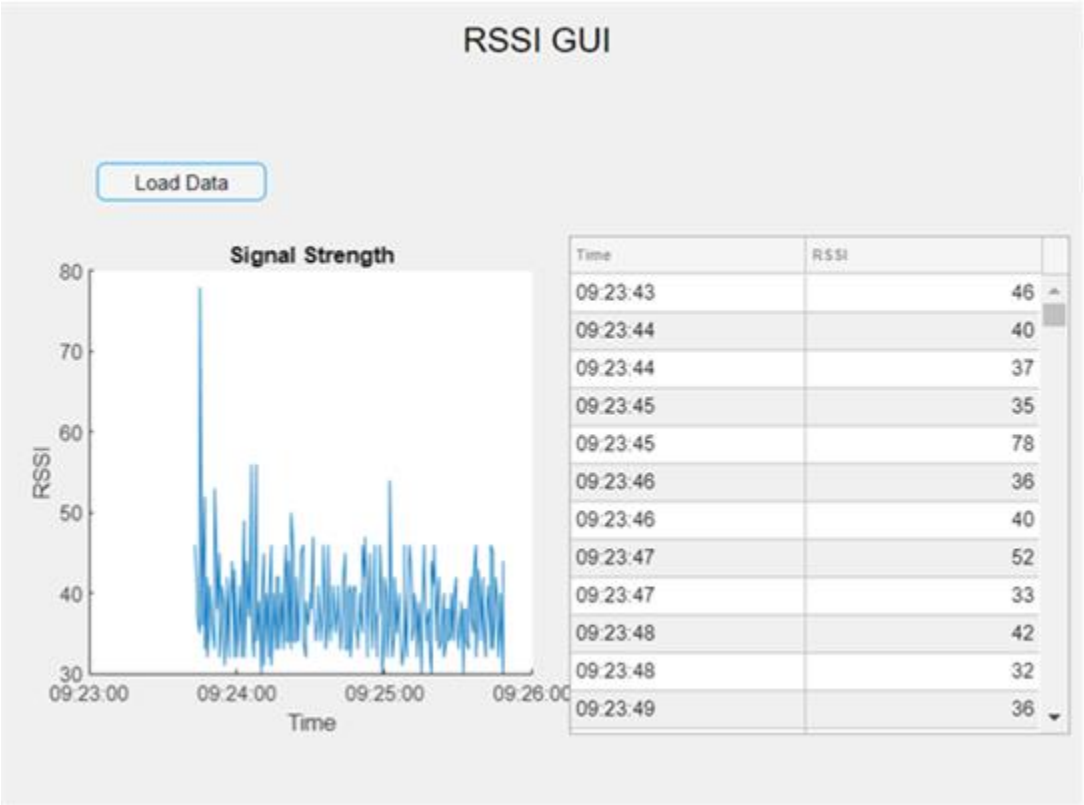

Figure 5.5: RSSI sample at 1m

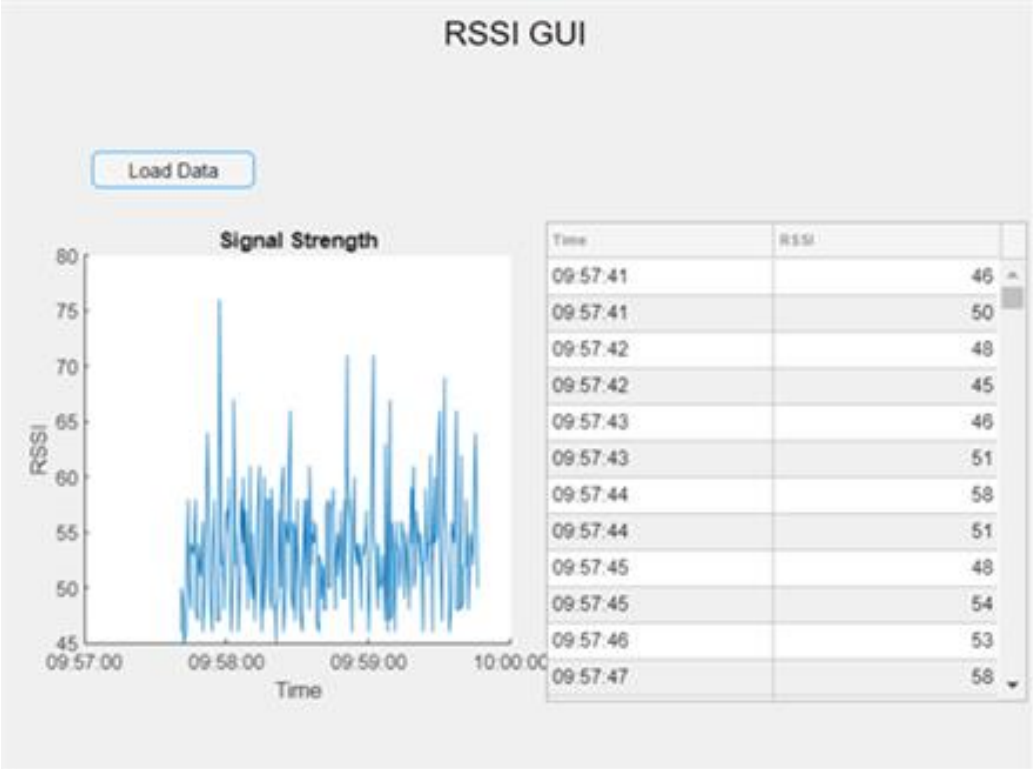

Figure 5.6: RSSI sample at 7m

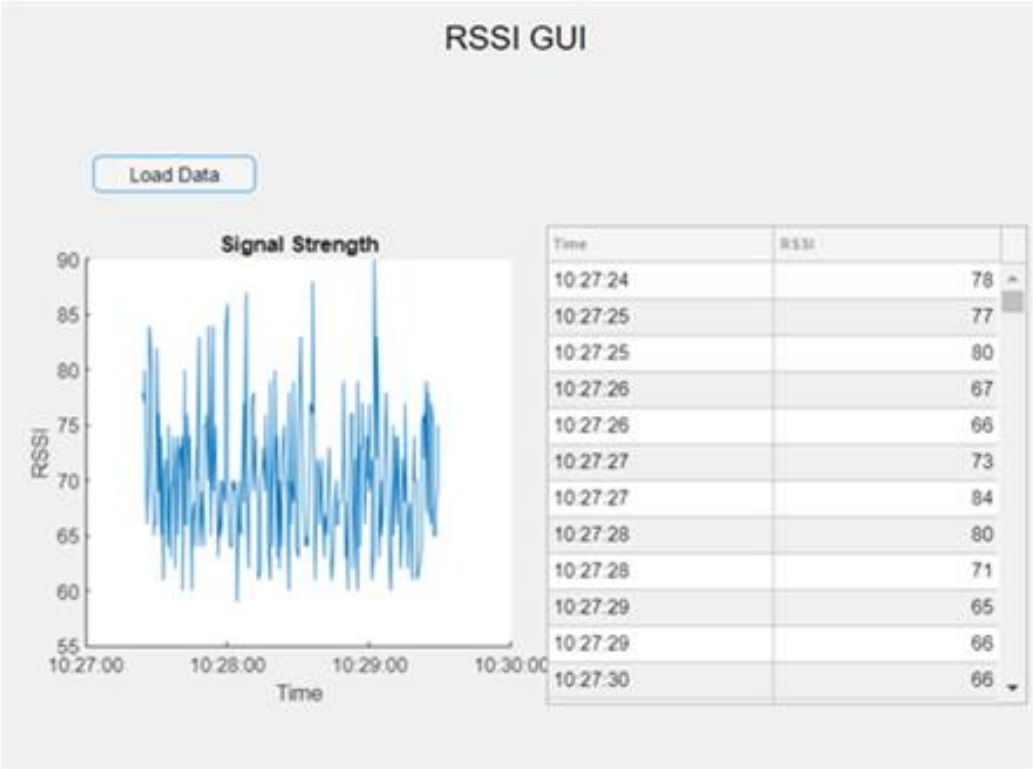

Figure 5.7: RSSI sample at 13m

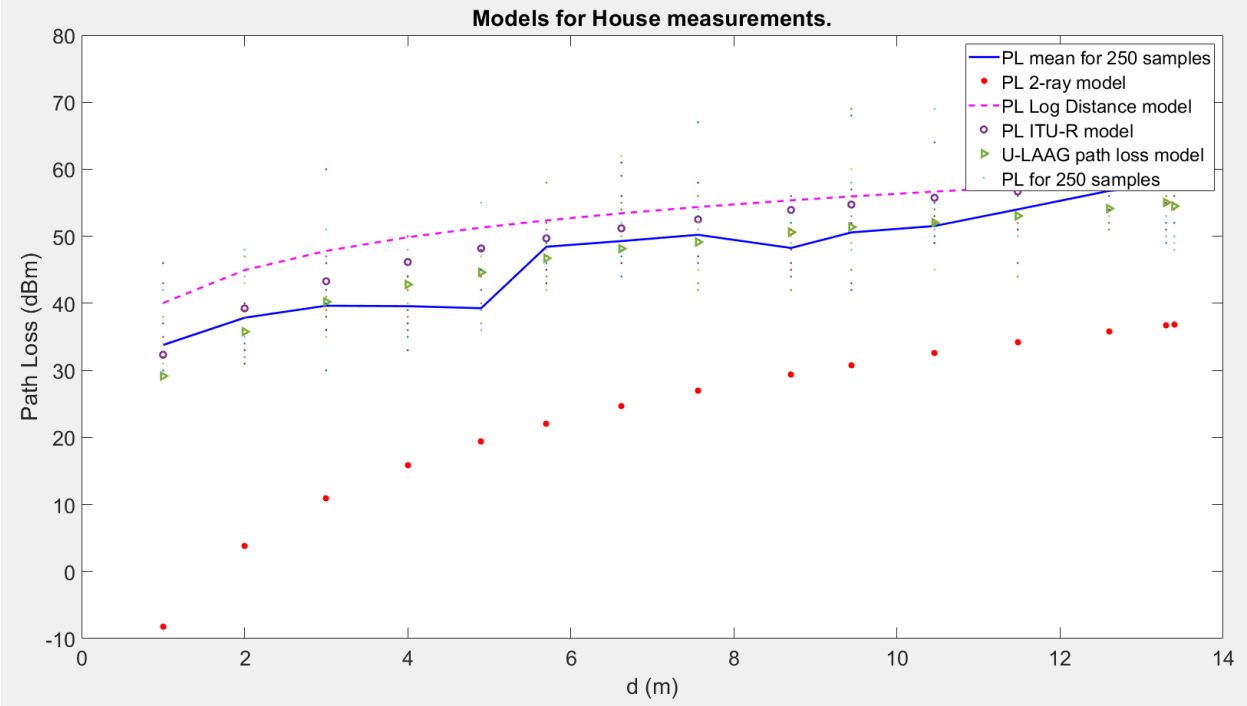

Figure 5.8: House experiment result

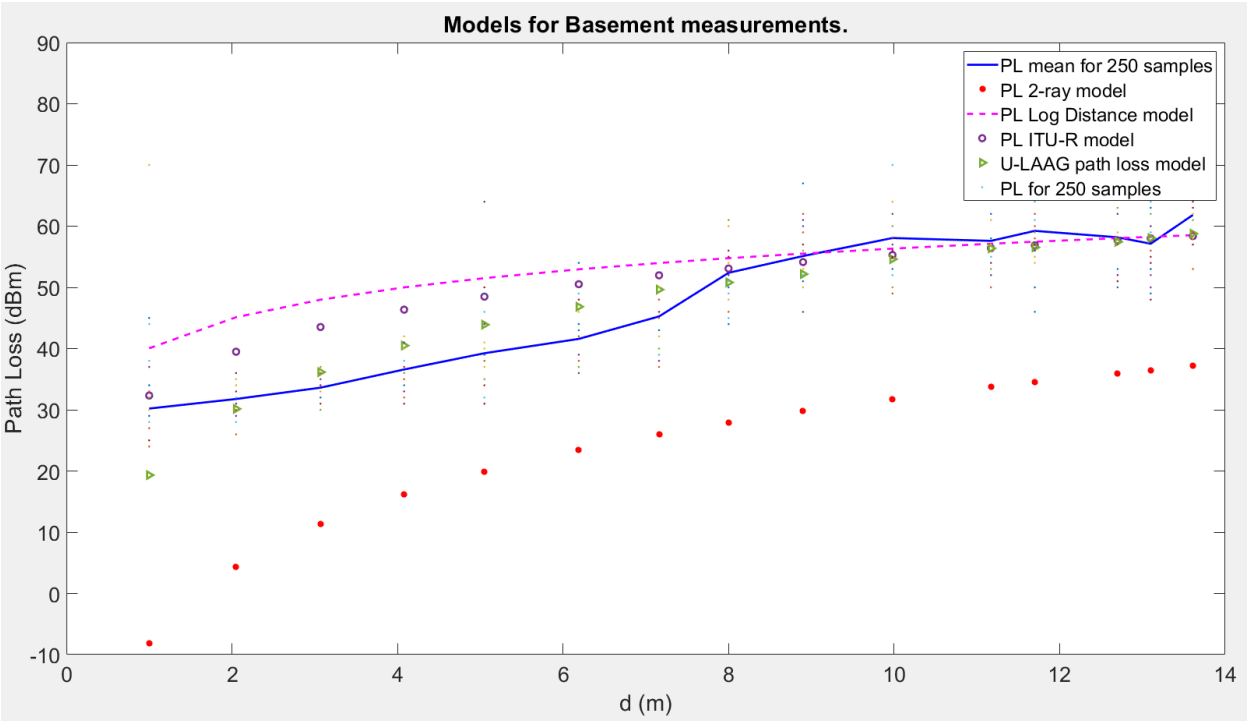

Figure 5.9: Basement experiment result

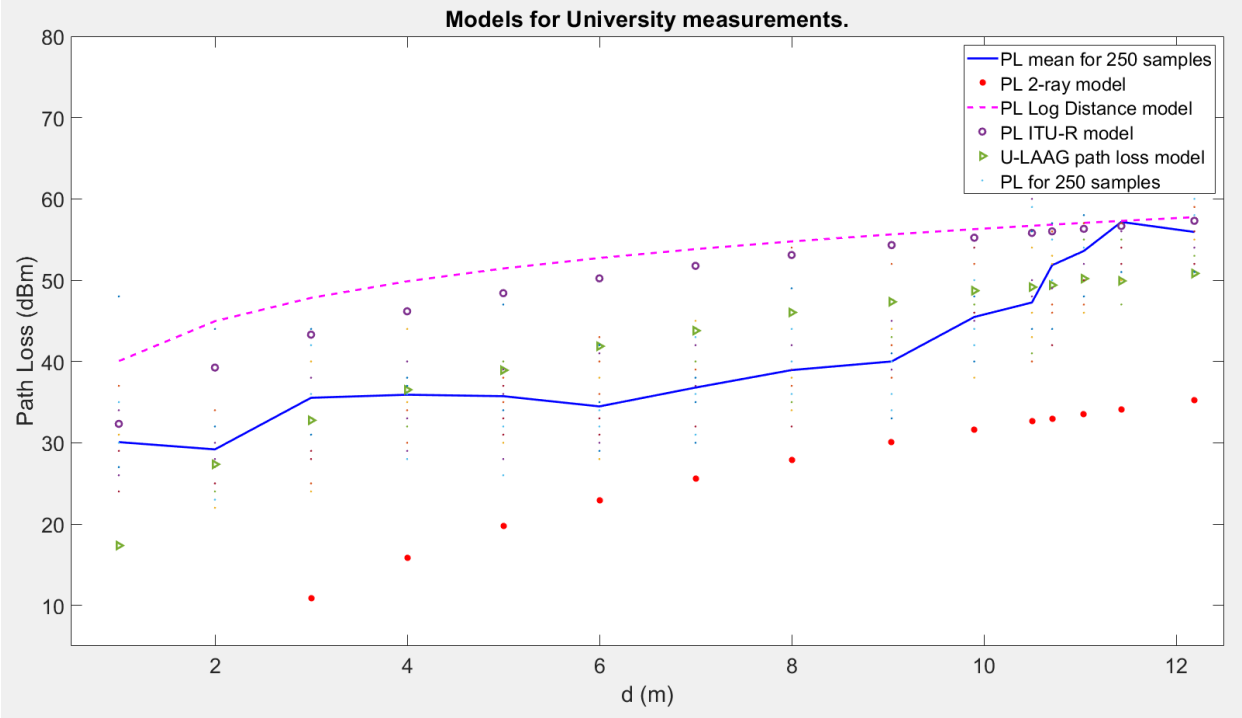

Figure 5.10: University experiment result

CHAPTER 6:
ANALYSIS OF MEASURED DATA

6.1: Two-ray Path Loss model measurement analysis

As discussed in section 2.1, the channel property is very important since it imposes constraints on the system's transmission rate, error probability and the distance over which the system can operate. This has prompted many recent experimental studies to suggest the use of a two-ray path loss model as a path loss baseline, with additional loss effects like shadowing caused by obstacles building on this [24]. We believe, however, that the use of the simplified Two-Ray Ground model as implemented in all major network simulation tools does not lead to a sufficient quality improvement. For the sake of completeness, two-ray path loss model is expressed as:

$$P_r(d) = \frac{\mathrm{P}_t \mathrm{G}_t \mathrm{G}_r \mathrm{h}_t^2 \mathrm{h}_r^2}{\mathrm{d}^4 \mathrm{L}} \tag{6.1}$$

Operating Parameter	Value
Transmission Power	8 dBm
Frequency Band	2.4 GHz
Coordinator height, h_{TX}	1.04 m
End device height, h_{RX}	1.52 m
Coordinator antenna gain, G_{TX}	2.1 dBi
End device antenna gain, G_{RX}	2.1 dBi

Table 6.1: Operating parameters for experiments

Based on early findings shown in [25] and from Table 6.2, we investigated the implemented path loss models in detail according to Table 6.1 parameters, and validated the results based on own experiments in an indoor environment using Digi Xbee3. We were able to analytically verify that simplified Two-Ray Ground models are of no benefit when simulated for any of the indoor environment (House, Basement, University), as shown in Figure 6.1 – 6.3. Table 6.2 shows the deviations experienced by two-ray path loss model.

Deviation \ Scenario	Minimum deviation (dBm)	Distance (m)	Maximum deviation (dBm)	Distance (m)
House	19.16	13	42.2	1
Basement	19.49	14	38.2	1
University Corridor	10.03	9	38.2	1

Table 6.2: Deviations for Two-ray path loss model

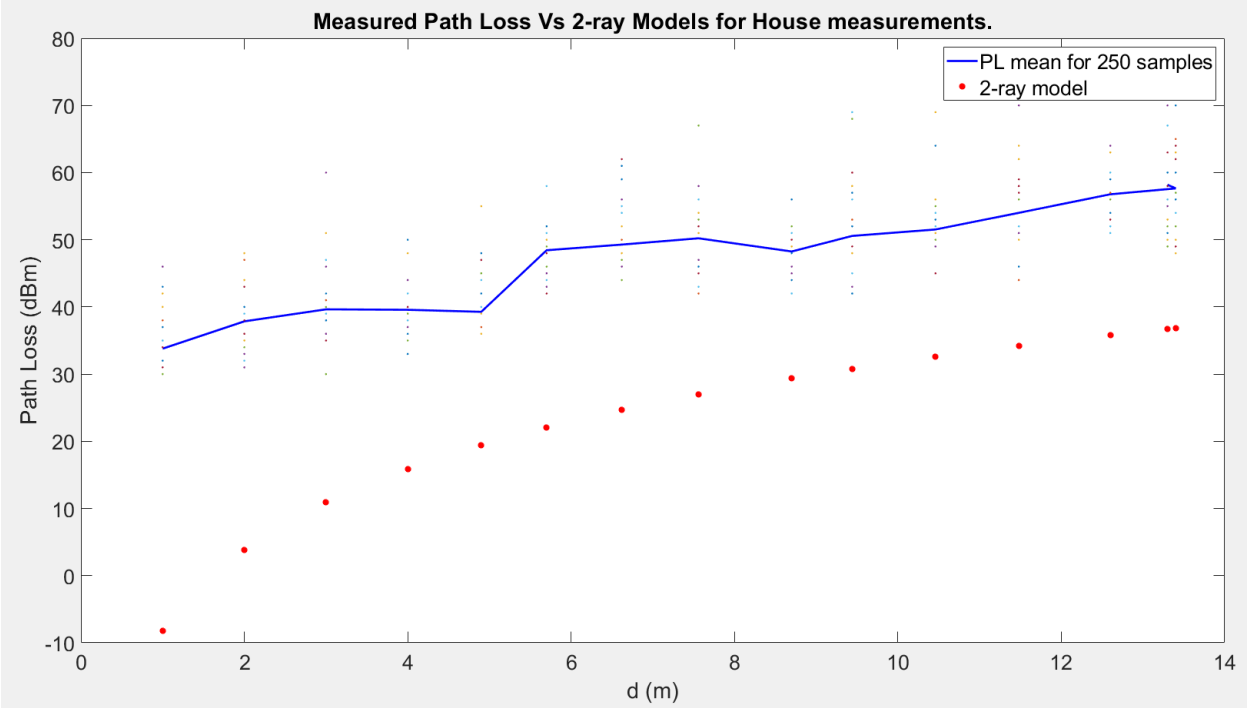

Figure. 6.1: Two-ray Path Loss model Vs. Measured Path Loss model for House measurements

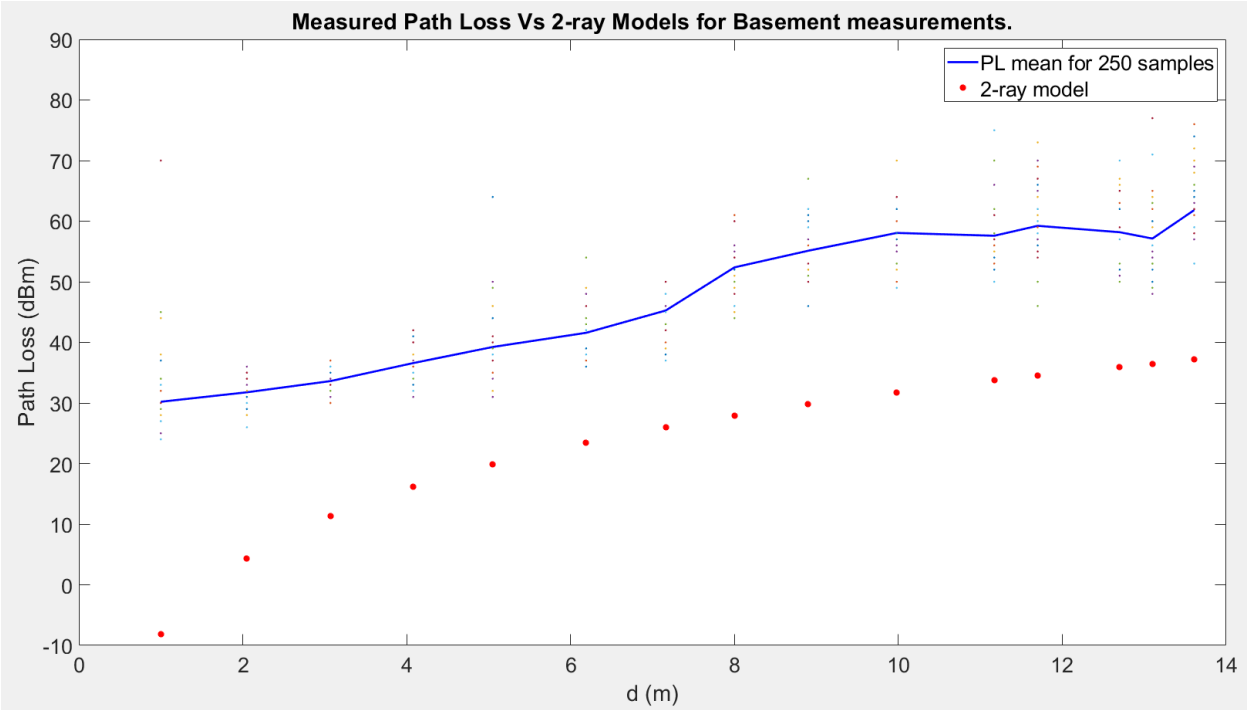

Figure. 6.2: Two-ray Path Loss model Vs. Measured Path Loss model for Basement measurements

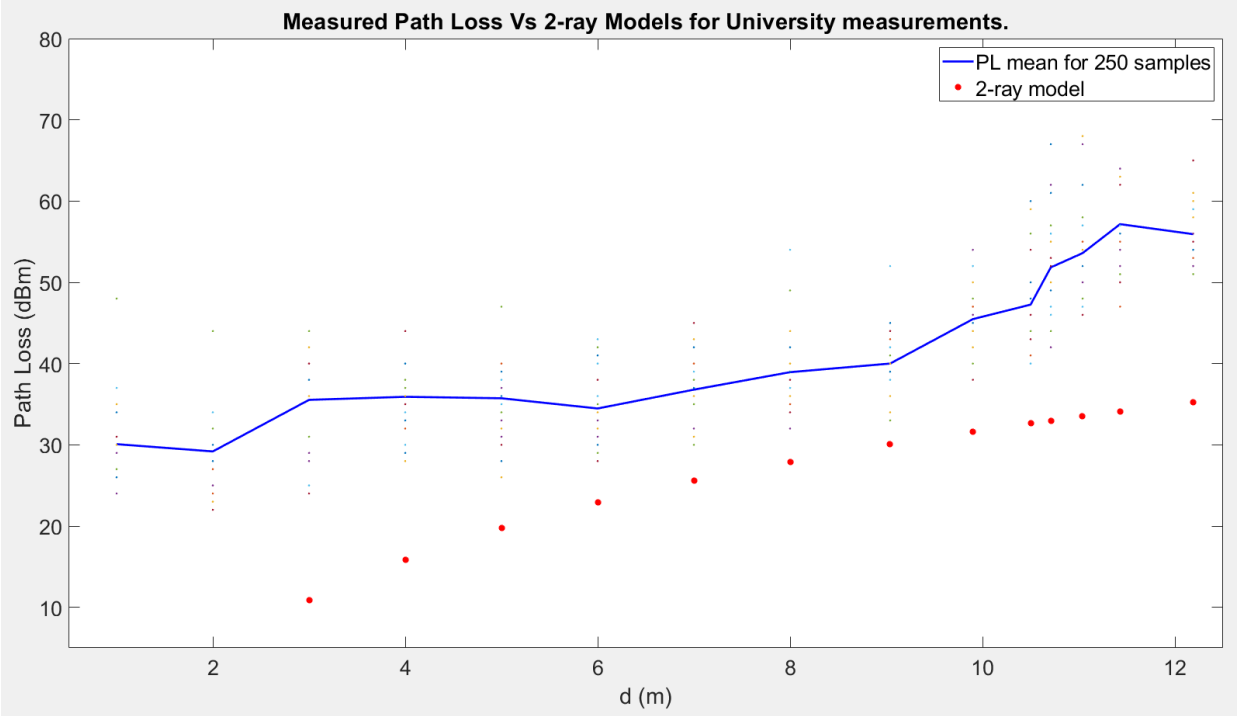

Figure. 6.3: Two-ray Path Loss model Vs. Measured Path Loss model for University corridor measurements

6.2: Log-Distance Path Loss model measurement analysis

We have simulated Log-distance model (Equation 6.2) according to parameters depicted in Table 6.3 for comparison.

$$\overline{PL}(dB) = \overline{PL}(\mathrm{d}_0) + 10.n.log\left(\frac{d}{d_0}\right) \qquad (6.2)$$

Operating parameter	Value
Transmission Power	8 dBm
Frequency Band	2.4 GHz
Reference distance, d_0	1 m
Total distance	(1 - 13) m
Path Loss exponent	1.63

Table 6.3: Parameters for Log-Distance model

From the results shown in Table 6.4, we were able to analytically verify that Log-Distance path loss model also fails to match out path loss model. As shown in plot Figures 6.4 – 6.6, we can conclude that a maximum deviation at lower distances (1m - 6m) and a minimum deviation at higher distances (8m - 13m) were experienced. For lower elevation scenarios, the model fits the data to an accuracy of 9dB after an approximate distance of 8m in all scenarios, while the model deviated from the data by 5dB-12dB at distance lower than 8m.

So, we can conclude that this model is not appropriate for our UAV take-off and landing scenarios, where both transmitter and receiver experience the same amount of scattering.

Deviation \ Scenario	Minimum deviation (dBm)	Distance (m)	Maximum deviation (dBm)	Distance (m)
House	1	13	13	5
Basement	0	13	14.21	3
University Corridor	1.73	14	18.26	6

Table 6.4: Deviations for Log-Distance path loss model

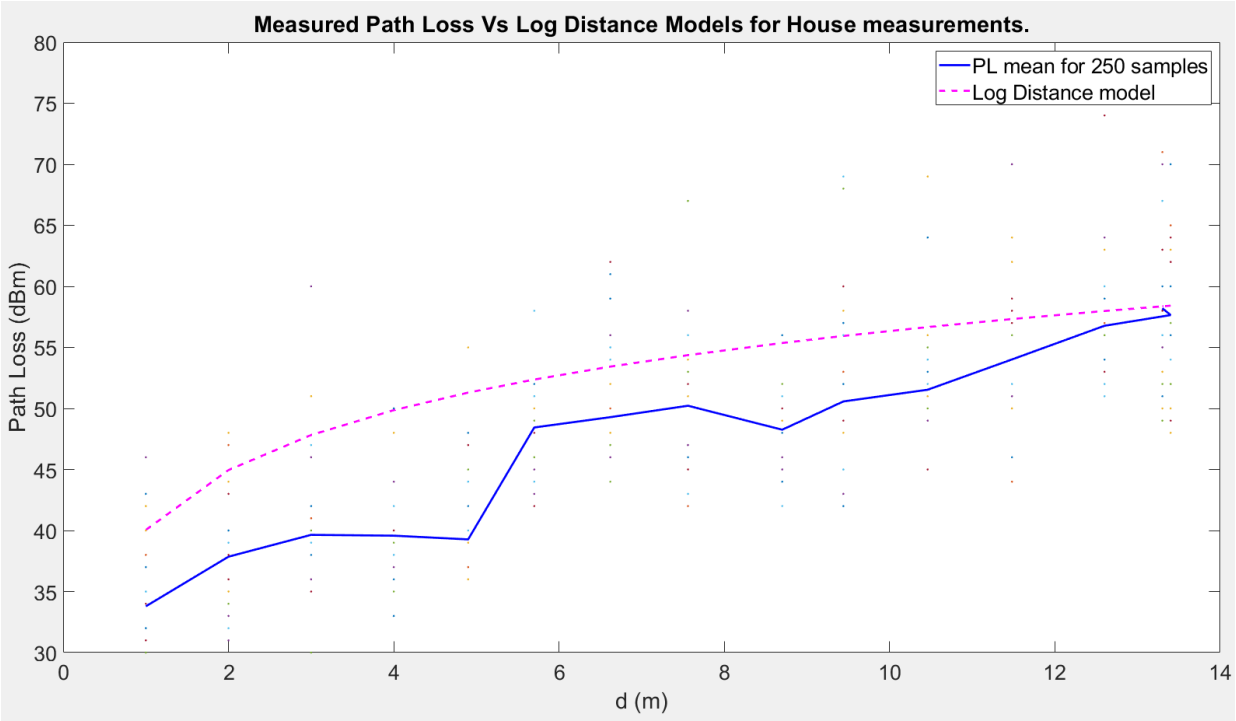

Figure. 6.4 Log-distance Path Loss model Vs. Measured Path Loss model for House measurements

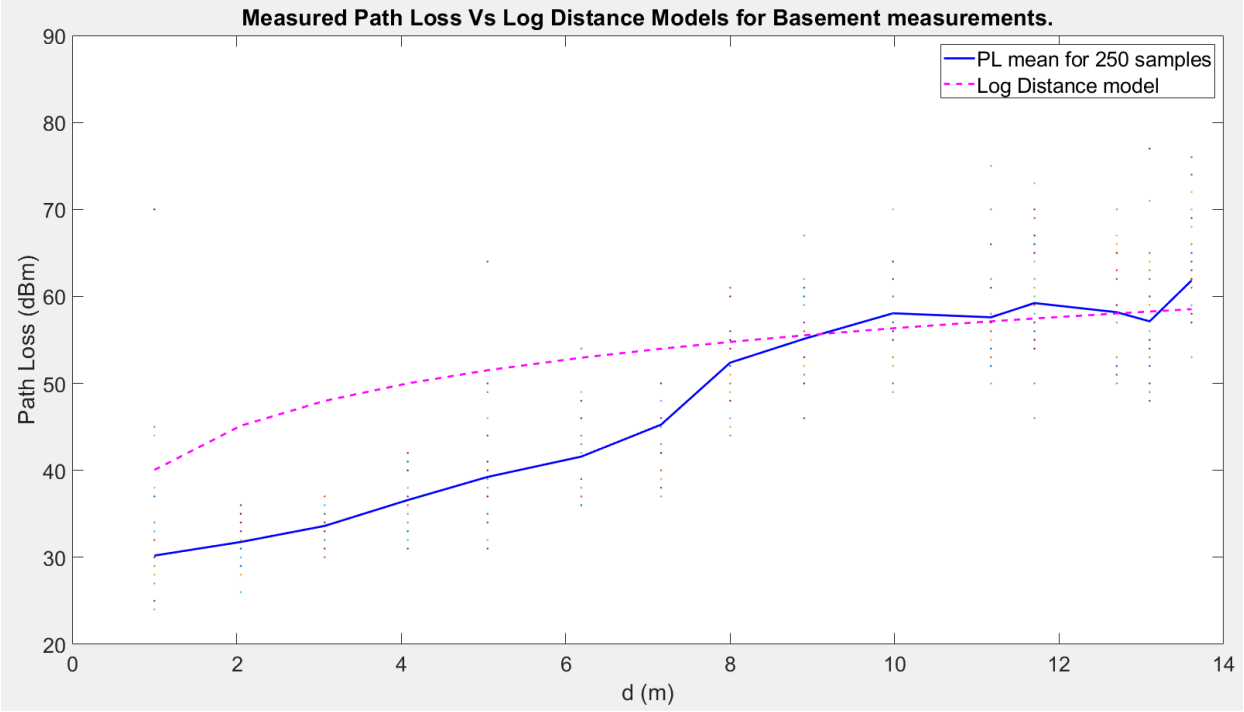

Figure. 6.5 Log-distance Path Loss model Vs. Measured Path Loss model for Basement measurements

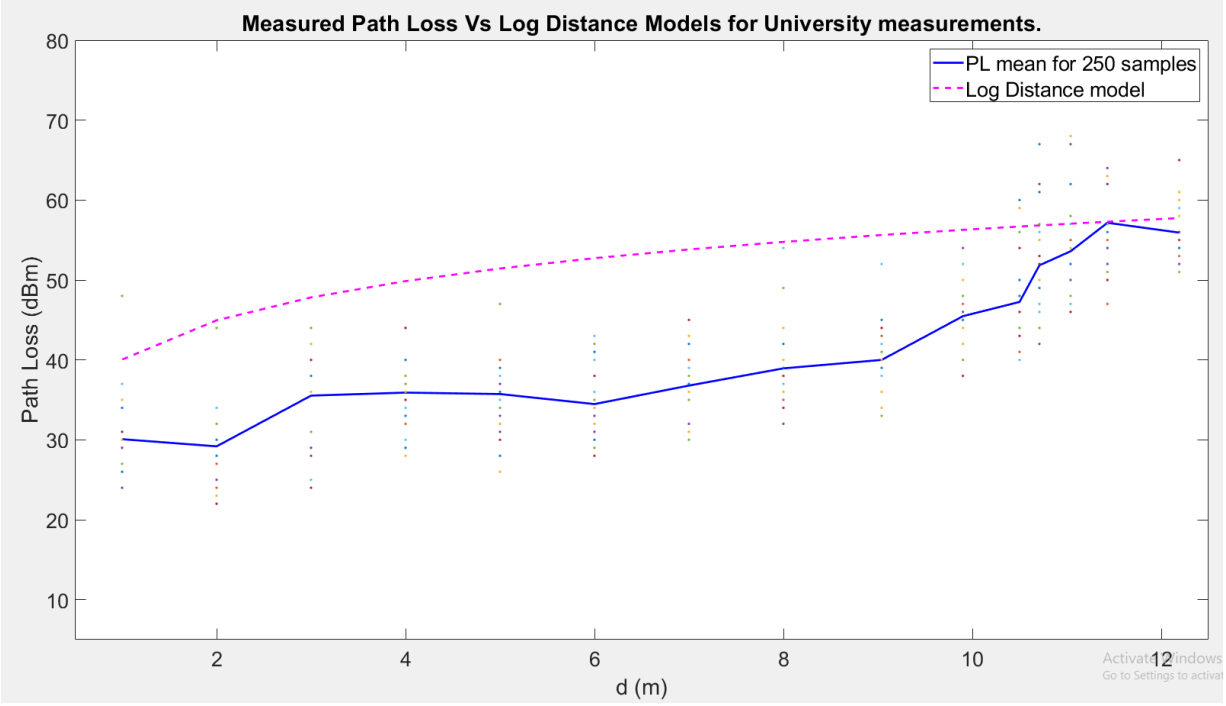

Figure. 6.6 Log-distance Path Loss model Vs. Measured Path Loss model for University corridor measurements

6.3: ITU-R model

The (International Telecommunication Union) ITU-R site-general model for path loss prediction in an indoor propagation environment is given by:

$$PL(dB) = 20\log_{10}(f) + N\log_{10}(d) + P_f(n) - 28 \quad (6.3)$$

Where N is the distance power decay index, f is the frequency in MHz, d is the distance in meters (d > 1m), $P_f(n)$ is the floor penetration loss factor and n is the number of floors between the transmitter and the receiver. Empirical value of N is used as 30, 28 and 22 for office, residential and commercial areas respectively.

Using curve-fitting model, we were able to minimize the deviation between our measured mean path loss model and ITU-R path loss model. For lower elevation scenarios, the model fits the data to an accuracy of 8dB after an approximate distance of 8m in all scenarios, while the model deviated from the data by 1dB-15dB at distance lower than 8m. From the simulations models shown in Figure 6.7 – 6.9 and results in Table 6.5, we can conclude that ITU-R model was the most successful model in matching with the measured mean Path Loss model. But there is still some room for improvement, as we will see in following section. As shown in plot Figures 6.7 – 6.9, we can conclude that a maximum deviation at lower distances (1m - 6m) and a minimum deviation at higher distances (8m - 13m) was experienced.

Deviation \ Scenario	Minimum deviation (dBm)	Distance (m)	Maximum deviation (dBm)	Distance (m)
House	1.15	13	9.12	5
Basement	0	13	9.58	4
University Corridor	1.69	14	15.75	6

Table 6.5: Deviations for ITU-R path loss model

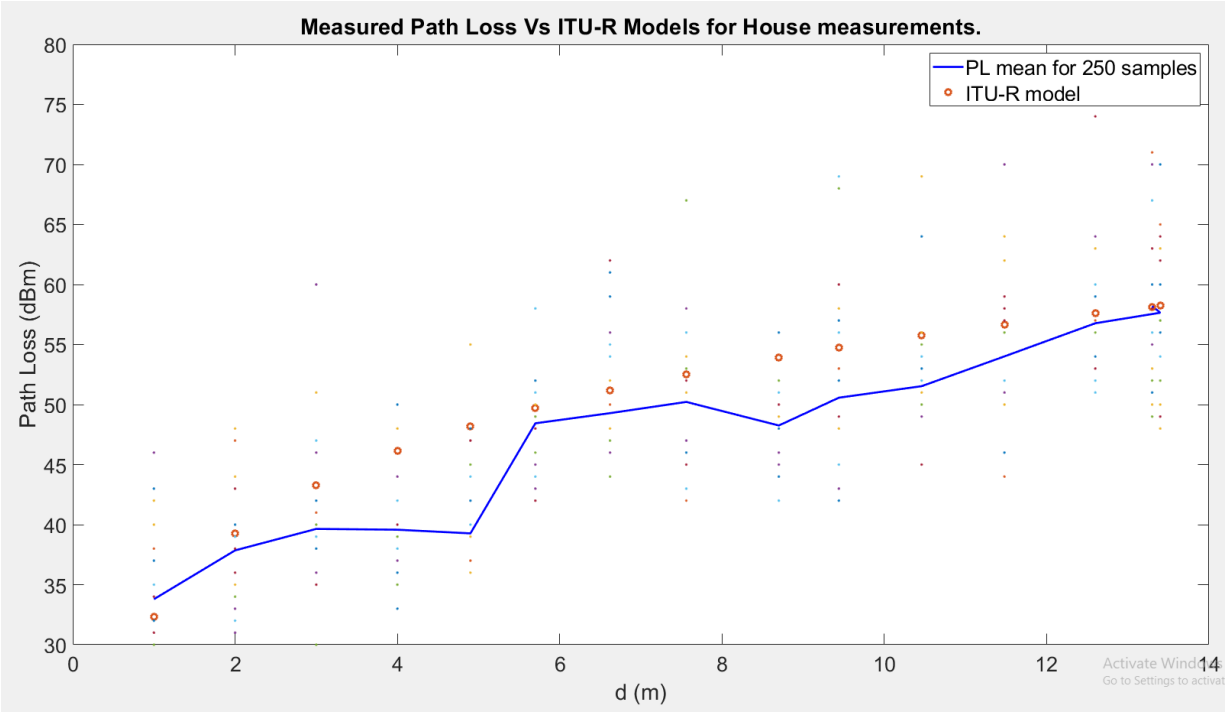

Figure. 6.7: ITU-R Path Loss model Vs. Measured Path Loss model for House measurements

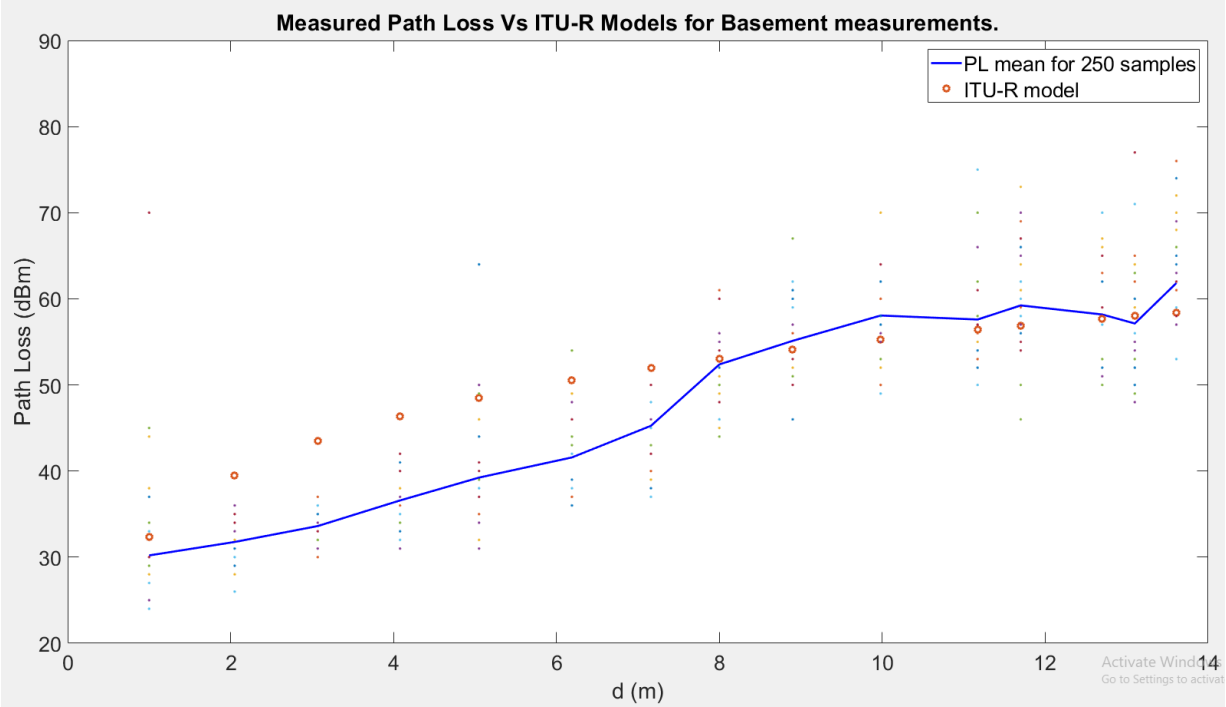

Figure. 6.8: ITU-R Path Loss model Vs. Measured Path Loss model for Basement measurements

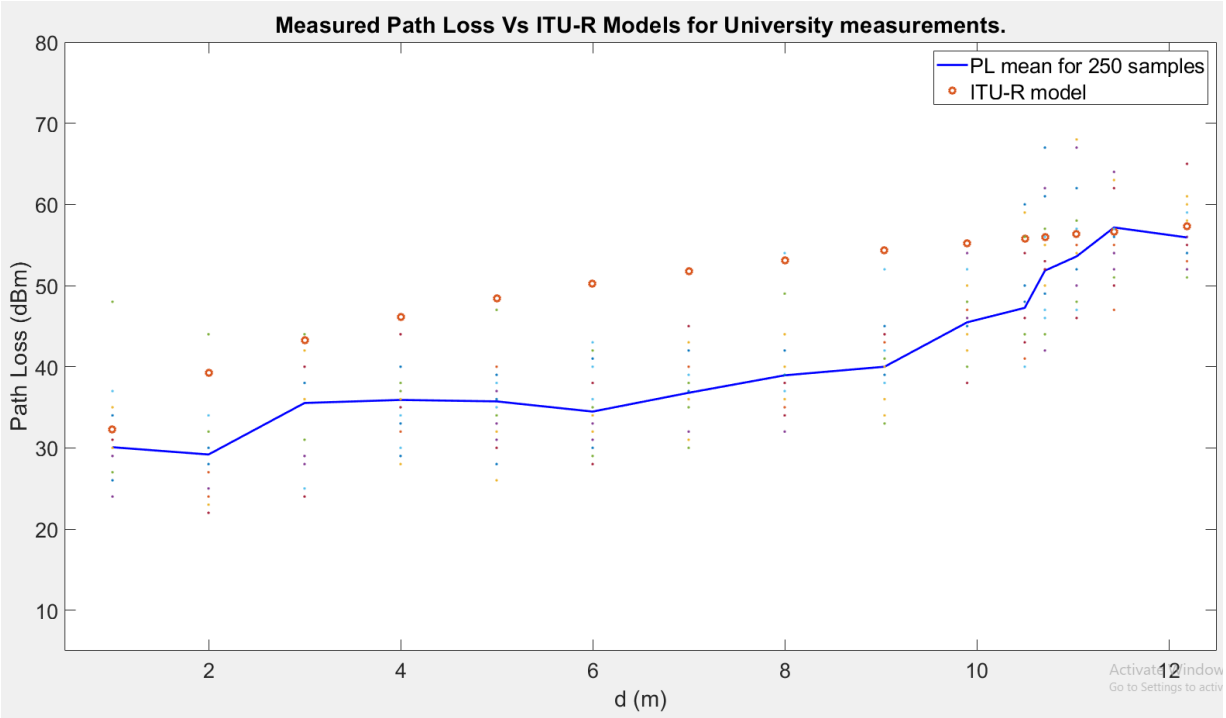

Figure. 6.9 ITU-R Path Loss model Vs. Measured Path Loss model for College corridor measurements

6.4: U-LAAG Path Loss model

As seen from the experiments of above described models, we can conclude that there is still a need for improvement in path loss models in an indoor environment at lower distances (1-8 m) from the base station. For the sake of completeness, U-LAAG model is expressed as:

$$PL_{U-LAAG}(dB) = 20.A.\log_{10} f_c + B.\log_{10} d + C + X_{sigma} \quad (6.4)$$

To evaluate the nature and correctness of our model U-LAAG, we have conducted the drive tests in three different scenarios, Home, Basement and University Corridor, and compared the proposed model with the experimental data. Figure 6.10, 6.11 and 6.12 illustrate the correctness of our model with the experimental data. It is to be noted that while conducting the experiment, we have not only moved the End-device in vertical direction to imitate a UAV landing and take-off scenario, but also made sure to create a NLOS condition for the signals to travel through the channel. From these figures, we observe that path loss values obtained by our proposed model are close to the average path loss values obtained from the experimental data.

We have used curve fitting techniques to obtain the constant parameter *C* as -1.5, used in our model. We have also observed from Table 6.6 that the value of parameters *A* and *B* differs for different scenario of operations. And to add shadowing effect to the

model, a zero-mean Gaussian random variable with standard deviation - σ is added to the equation.

Parameter \ Scenario	Home	Basement	University Corridor
A	0.16	0.11	0.10
B	22.85	34.6	30.78
C	-1.5	-1.5	-1.5
$X_{\text{Standard deviation}}$	1	1	1

Table 6.6: Estimated parameters of U-LAAG model

As shown in experiment model plots from Figures 6.10-6.12 and the results expressed in Table 6.7, we can conclude that a maximum deviation at lower distances (1-6 m) and a minimum deviation at higher distances (8-13 m) were experienced. As evident from the results shown below, we can conclude that a lower deviation was experienced in our model when compared with other models discussed above, at lower distances. And apparently the same pattern was seen at larger distances too. For lower elevation scenarios in a UAV, the model fits the data to an accuracy of 5dB at both higher and lower distances. So after a curve fitting method, U-LAAG model fits the data with a better accuracy when compared to other models described above. This model follows the same deviation pattern not only at larger distances, but at smaller distances too, making it the optimal model in such scenarios.

Deviation \ Scenario	Minimum deviation (dBm)	Distance (m)	Maximum deviation (dBm)	Distance (m)
House	0	12	5.73	5
Basement	0	13	5	5
College Corridor	0.4	4	7.06	6

Table 6.7: Deviations for U-LAAG path loss model

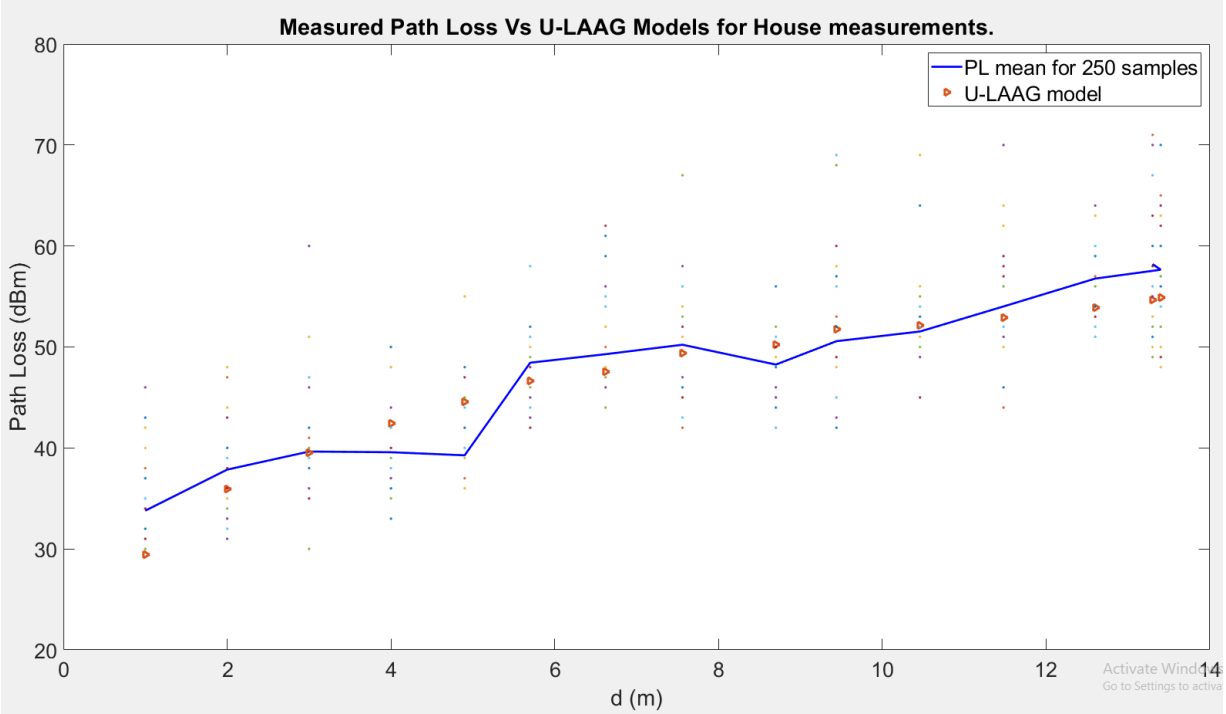

Figure. 6.10: U-LAAG Path Loss model Vs. Measured Path Loss model for House measurements

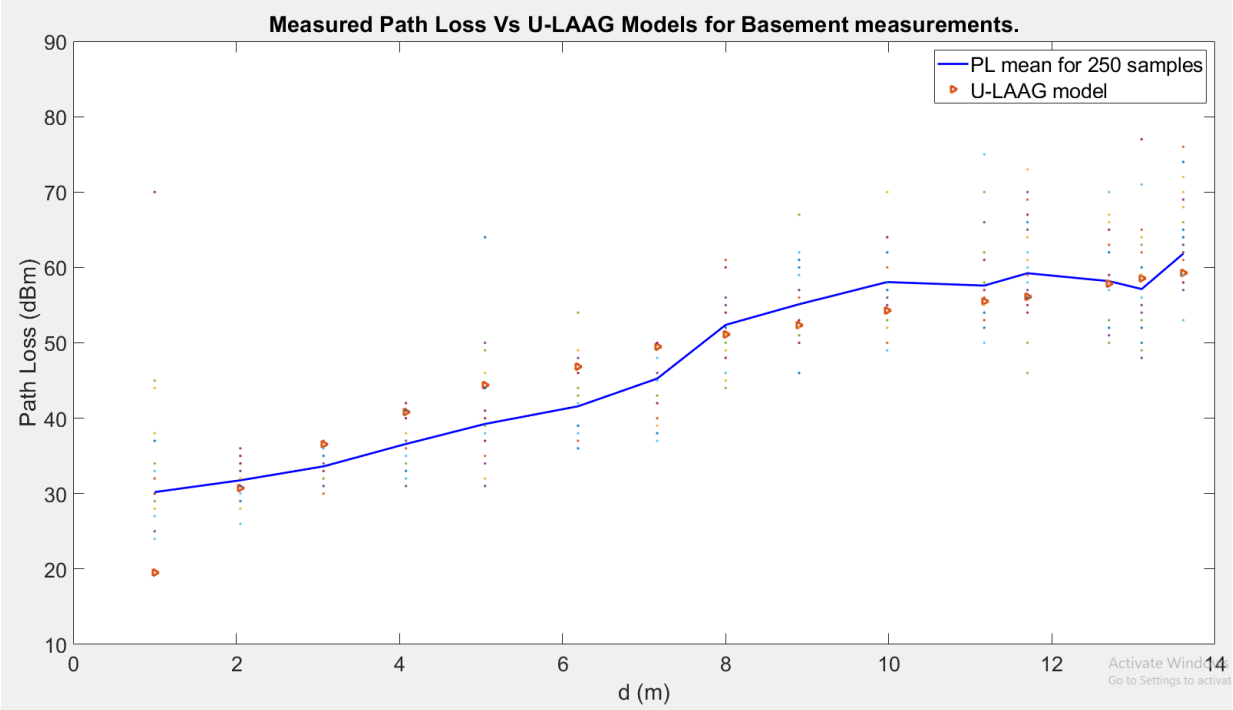

Figure. 6.11: U-LAAG Path Loss model Vs. Measured Path Loss model for Basement measurements

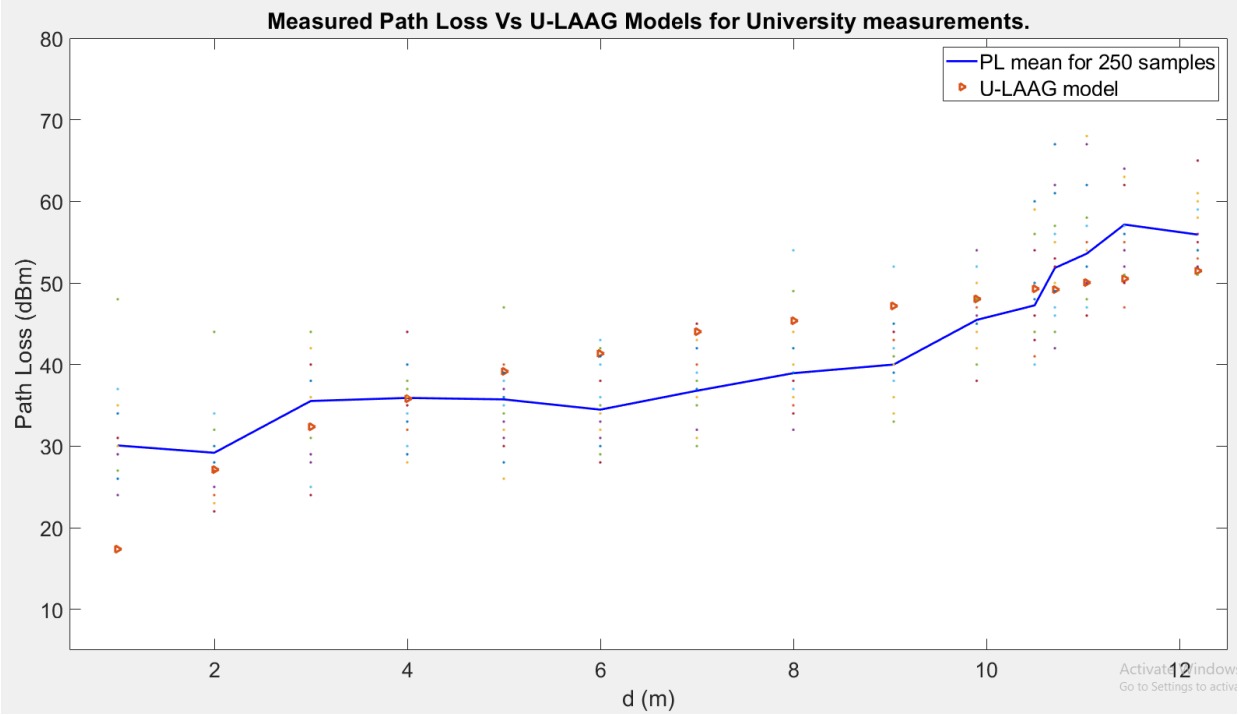

Figure. 6.12: U-LAAG Path Loss model Vs. Measured Path Loss model for University Corridor measurements

CHAPTER 7:
DISCUSSIONS BASED ON NEW MODEL PARAMETERS

7.1: Discussions Based On New Model Parameters

From all these scenarios, we observe that the value of parameter *B* differs significantly for each scenario; for Home: $B = 22.85$, for Basement: $B = 34.6$ and for University Corridor: $B = 30.78$. Our model is closely matching the observed path loss values in a close space, experiencing lot of scattering at both the ends. Value of parameter *A* obtained from our drive test data ranges from 0.10 to 0.16. From the House, Basement and University premises experiment, we have observed that the parameter *A* is significantly higher for house as compared to Basement and University premises. This is mainly because of the multi-path propagation and reflections that becomes inevitable in House scenario. We have used curve fitting techniques to obtain the constant parameter *C* as -1.5, used in our model. We have also observed from Table 5.6 that the value of parameters *A* and *B* differs for different scenario of operations. Parameters A, B and C reflect the directionality gain when the height of the antenna is varied at the receiver end from 0-1.5m to imitate the take-off and landing scenario of a UAV. And to add shadowing effect to the model, a zero-mean Gaussian random variable with standard deviation - σ is added to the equation.

We have also compared our proposed model U-LAAG with that of ITU-R, Log-distance and Two-ray path loss model. From the Figures 6.10-6.12, we have observed that our model matches closer with the experiment data as compared to other models.

7.2: Discussions from experiment data, proposed model and the existing models (ITU-R, Two-ray and Log-distance)

The deviation between the mean observed path loss and our proposed path loss values varies between 0.4-7.06 dBm; as seen from the Figures 6.10-6.12, minimum in the basement and maximum in the University corridor. The basement acted as uniform environment with least amount of uneven placed objects, and a good amount of contact with the ground surface. These were few of the reasons due to which a minimum amount of deviation was experienced by our model. And the same characteristic was followed by other models too. The house and university environment had a lot of non-uniformities in their setup, due to the uneven placement of random objects with different reflecting properties. This setup acted as a realistic environment, to see the applicability of our model, experiencing the maximum amount of deviation from the mean observed path loss model.

The deviation between the mean observed path loss and Log-distance model varies between 1 - 18.26 dBm; minimum at larger distances (beyond 13m) and maximum in the closer distances (0-6 m), as seen from the Figures 5.5-5.7. Similarly, deviation of 10.03-42.2 dBm was observed in the case of Two-ray path loss model (Figures 6.1-6.3). Both models, Two-ray and Log distance path loss model were unable to match the

observed path loss model, even after the curve fitting method. These models are a good fit for comparison purposes, but not for practical usage. Similarly, deviation of 1.15-15.75 dBm was observed in the case of ITU-R path loss model, after the curve fitting method. We observe that ITU-R model almost intersects with observed mean path loss model at larger distances, as seen in the Figures 6.7-6.9. So we believe that ITU-R is statistically a better model when compared to Two-ray and Log-distance path loss model.

When compared with our proposed model U-LAAG, we were able to achieve even less deviation 0.4-7.06 dBm, after the curve fitting method. We therefore argue that U-LAAG model can be used as a better estimator of path loss for indoor environment for the band 2.4GHz in a UAV take-off and landing scenarios at shorter distances.

CHAPTER 8:
CONCLUSIONS

In this report, we proposed an indoor average path loss model called UAV Low Altitude Air to Ground (U-LAAG) Model which can be used for regular UAV operations for the band 2.4 - 2.5 GHz in warehouse and industries. There was no work done on accurate models for low elevation scenarios corresponding to take-off, landing and closed indoor spaces. Based on several experiments conducted in a typical house environment, we have formulated a mathematical model which can be used in - indoor area, corridors, basement, etc. This is an accurate model for lower elevations in an indoor environment. We have also compared U-LAAG with popular path loss models used in practice such as ITU-R, Two-ray and Log-distance model and have demonstrated the correctness of our model. This model can be suitably extended to other countries through rigorous experiments. Due to its adaptive nature, U-LAAG can be used for regular indoor IoT deployment and robotics operating in 2.4 - 2.5 GHz to achieve an accurate simulation and planning of power consumption link budget for reliable communication.

CHAPTER 9:
FUTURE WORK

As a part of future work, we recommend to extend path loss models for other frequency bands such as 5.8 GHz for regular Wi-Fi and mm Wave frequencies in mines, tunnels, warehouse, factories, University seminar halls, etc., to achieve lower latency. There were few limitations in this work, which can be extended in future. Due to the COVID-19 pandemic, my work was limited to the environments accessible to me. So this experiment model can be tested for various environments discussed above. And For getting more accurate data, the work can be extended with real drones in their take-off and landing scenarios, and to multi-floor scenarios.

REFERENCES

[1] International Telecommunications Union, "Characteristics of Unmanned Aircraft Systems and Spectrum Requirements to Support their Safe Operation in Non-Segregated Airspace," ITU-R M.2171, December 2009.

[2] D. W. Matolak, "Air-Ground Channels & Models: Comprehensive Review and Considerations for Unmanned Aircraft Systems," IEEE Aerospace Conference, Big Sky, MT, 3-10 March 2012.

[3] D. W. Matolak, R. Sun, "Air-Ground Channel Characterization for Unmanned Aircraft Systems—Part I: Methods, Measurements, and Results for Over-water Settings," IEEE Trans. Veh. Tech., (online 2016), vol. 66, no. 1, pp. 26-44, Jan. 2017.

[4] R. Sun, D. W. Matolak, "Air-Ground Channel Characterization for Unmanned Aircraft Systems—Part II: Hilly & Mountainous Settings," IEEE Trans. Veh. Tech., vol. 66, no. 3, pp. 1913-1925, March 2017.

[5] D. W. Matolak, R. Sun, "Air-Ground Channel Characterization for Unmanned Aircraft Systems—Part III: The Suburban and Near-Urban Environments," IEEE Trans. Veh. Tech., vol. 66, no. 8, pp. 6607-6618, August 2017.

[6] D. W. Matolak, Uwe-Carsten Fiebig, "UAV Channel Models: Review and Future Research" 13th European Conference on Antennas and Propagation (EuCAP 2019)

[7] W. G. Newhall, R. Mostafa, C. Dietrich, C. R. Anderson, K. Dietze, G. Joshi, and J. H. Reed, "Wideband air-to-ground radio channel measurements using an antenna array at 2 GHz for low-altitude operations," in Proc. IEEE Military Commun. Conf. (MILCOM), vol. 2, 2003, pp. 1422–1427.

[8] H. D. Tu and S. Shimamoto, "A proposal of wide-band air-to-ground communication at airports employing 5-GHz band," in Proc. IEEE Wireless Commun. Networking Conf. (WCNC), 2009, pp. 1–6.

[9] D. W. Matolak and R. Sun, "Air-ground channel characterization for unmanned aircraft systems: The near-urban environment," in Proc.

[10] D. W. Matolak and R. Sun, "Antenna and frequency diversity in the unmanned aircraft systems bands for the over-sea setting," in Proc. IEEE Digital Avionics Sys. Conf. (DASC), Oct. 2014, pp. 6A4–1–6A4–10.

[11] D. W. Matolak, "Channel characterization for unmanned aircraft systems," in Proc. European Conf. Ant. Propag. (EuCAP), 2015, pp. 1–5.

[12] US Department of Transportation Federal Aviation Authority, “Integration of Civil Unmanned Aircraft Systems (UAS) in the National Airspace System (NAS) Roadmap," 2013, available online at http://www.faa.gov/uas/media/uas_roadmap_2013.pdf.

[13] Civil Aviation Safety Authority (CASA), “Flying drones or model aircraft recreationally”, available online at https://www.casa.gov.au/modelaircraft.

[14] M. Simunek, F.P. Fontan, and P. Pechac, “The UAV Low Elevation Propagation Channel in Urban Areas: Statistical Analysis and Time-Series Generator," IEEE Trans. Antennas Propag., vol. 61, no. 7, pp. 3850-3858, 2013.

[15] M. Simunek, P. Pechac, and F.P. Fontan, “Excess Loss Model for Low Elevation Links in Urban Areas for UAVs," Radio engineering, vol. 20, no. 3, pp. 561-568, 2011.

[16] M. Simunek, F.P. Fontan, P. Pechac, and F.J.D. Otero, “Space Diversity Gain in Urban Area Low Elevation Links for Surveillance Applications," IEEE Trans. Antennas Propag., vol. 61, no. 12, pp. 6255-260, 2013.

[17] M. Simunek, P. Pechac, and F.P. Fontan, “Feasibility of UAV Link Space Diversity in Wooded Areas," Intl. J. Antennas Propag., vol. 2013, pp. 1-6,2013.

[18] Aziz Altaf Khuwaja, Yunfei Chen, Nan Zhao, Mohamed-Slim Alouini, Paul Dobbins, “A Survey of Channel Modeling for UAV Communications”, IEEE Communications Surveys & Tutorials (Volume: 20 , Issue: 4 , Fourthquarter 2018)

[20] S. Zvinovec, M. Vlek, and P. Pechac, “Results of Indoor Propagation Measurement Campaign for WLAN Systems Operating in 2.4 GHz ISM Band,” in Antennas and Propagation-ICAP03, vol. 1, pp. 63–66, 2003.

[21] C. C. Monti, M. Vari, and F. Mazzenga, “Path Loss Models for IEEE 802.11a Wireless Local Area Networks,” 3rd International Symposium on Wireless Communication Systems-ISWCS06, pp. 621 – 624, 2006.

[22] E. Tanghe, W. Joseph, L. Verloock, L. Martens, H. Capoen, K. V. Herwegen, and T. Buysschaert, “Range of an IEEE 802.11b/g system in industrial environments based on site survey measurements and propagation models,” in Proc. of the Antennas and Propagation Society International Symposium, 2008.

[23] T. S. Rappaport, “Wireless Communications Principles & Practice,” Prentice Hall Inc., vol. 2, 1996.

[24] T. Chrysikos, G. Georgopoulos, and S. Kotsopoulos, “Site-specific validation of ITU indoor path loss model at 2.4 GHz,” in World of Wireless, Mobile and Multimedia Networks and Workshops, pp. 329 – 334, 2011.

[25] T. Chrysikos, G. Georgopoulos, and S. Kotsopoulos, “Attenuation over distance for indoor propagation topologies at 2.4 GHz,” in IEEE Symposium on Computers and Communications (ISCC), pp. 1 – 6, 2009.

[26] S. M. Hameed, “Indoor Propagation Modeling for Wireless Local Area Network (WLAN),” IJCCCE, vol. 11, no. 1, pp. 97–105, 2011.

[27] J. W. Lim, Y. S. Shin, and J. G. Yook, “Experimental performance analysis of IEEE802.11a/b operating at 2.4 and 5.3 GHz,” in The 2004 Joint Conference of the 10th Asia-Pacific Conference on Communications, pp. 133 – 136, 2004.

Appendix A: XBee3 pinout

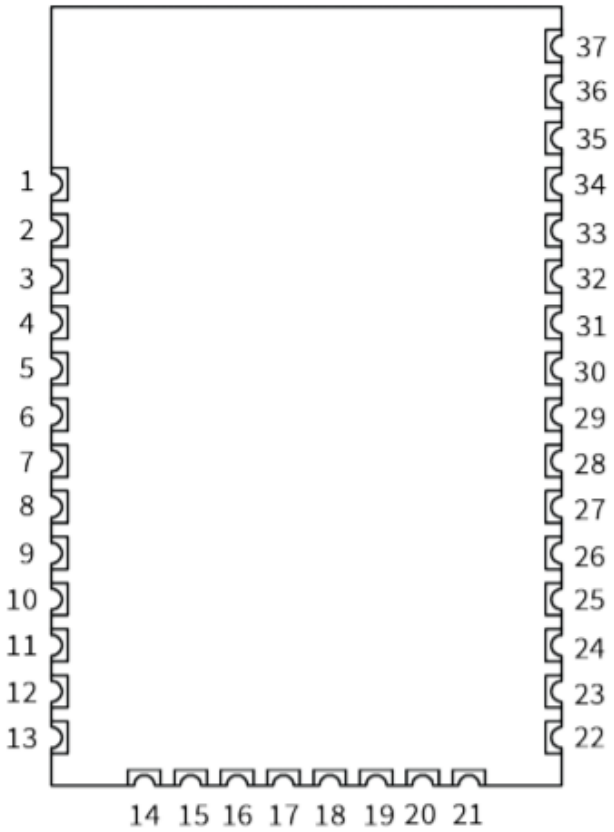

Pin #	Name	Default State	Description
1	GND	-	Ground
2	VCC	-	Power supply
3	DOUT /DIO13	Output	UART data out /GPIO
4	DIN / CONFIG /DIO14	Input	UART data in /GPIO
5	DIO12	-	GPIO
6	RESET	-	Device reset.
7	RSSI PWM/DIO10	Output	RX signal strength

			Indicator /GPIO.
8	PWM1/DIO11/I2C SDA	Disabled	Pulse width modulator/GPIO/I2C SDA.
9	[reserved]	Disabled	Do not connect.
10	DTR/SLEEP_RQ /DIO8	Input	Pin sleep control Line/GPIO
11	GND	-	Ground
12	SPI_ATTN/ BOOTMODE /DIO19	Output	Serial peripheral interface attention . Do not tie low on reset.
13	GND	-	Ground
14	SPI_CLK /DIO18	Input	Serial peripheral interface clock/GPIO
15	SPI_SSEL/DIO17	Input	Serial peripheral interface not select/GPIO
16	SPI_MOSI/DIO16	Input	Serial peripheral interface data in/GPIO
17	SPI_MISO/DIO15	Output	Serial peripheral interface data out/GPIO
18	[reserved]	Disabled	Do not connect
19	[reserved]	Disabled	Do not connect
20	[reserved]	Disabled	Do not connect
21	[reserved]	Disabled	Do not connect
22	GND	-	Ground
23	[reserved]		Do not connect
24	DIO4	Disabled	GPIO

25	CTS/DIO7	Output	Clear to send flow control/GPIO
26	ON/SLEEP/DIO9	Output	Device status indicator/GPIO
27	[reserved]	Disabled	Do not connect or connect to Ground.
28	ASSOCIATE/DIO5	Output	Associate Indicator/GPIO
29	RTS/DIO6	Input	Request to send flow control /GPIO
30	AD3/DIO3	Disabled	Analog input/GPIO.
31	AD2/DIO2	Disabled	Analog input/GPIO.
32	AD1/DIO1/I2C SCL	Disabled	Analog input/GPIO/I2C SCL
33	AD0 /DIO0	Input	Analog input / GPIO / Commissioning button
34	[reserved]	Disabled	Do not connect
35	GND	-	Ground
36	RF	-	RF I/O for RF pad variant
37	[reserved]	Disabled	Do not connect

Appendix B: Grove Connector pinout

	Pinout	Signal	Comments
Grove DIO12	1	DIO12	
	2	-	
	3	3.3V	
	4	GND	
Grove DIO14	1	DIO4	Signal connected to the LED/button
	2	-	
	3	3.3V	
	4	GND	
Grove AD0	1	AD0/CB	Signal connected to the commissioning button
	2	-	
	3	3.3V	
	4	GND	
Grove AD3	1	AD3	
	2	-	
	3	3.3V	
	4	GND	
Grove I2C	1	DIO1/I2C_SCL	
	2	DIO11/I2C_SDA	
	3	3.3V	
	4	GND	

Grove PWM0	1	RSSI/PWM0	Signal connected to the RSSI LED
	2	-	
	3	3.3V	
	4	GND	
Grove DIO19	1	DIO19	
	2	-	
	3	3.3V	
	4	GND	
Grove DIO18	1	DIO18	
	2	-	
	3	3.3V	
	4	GND	